Journal of Applied Fluid Mechanics, Vol. 18, No. 11, pp. 2659-2679, 2025.
Available online at www.jafmonline.net, ISSN 1735-3572, EISSN 1735-3645.
https://doi.org/10.47176/jafm.18.11.3448

Investigation of Heaving-pitching Airfoil in Ground Proximity using Large Eddy Simulations

Y. E. William[1], S. Kanagalingam[2,3] and M. H. Mohamed[4,5†]

[1] *Department of Mechanical Engineering, National University of Singapore, Singapore*
[2] *School of Mechanical and Aerospace Engineering, Nanyang Technological University, Singapore*
[3] *Department of Aerospace and Geodesy, Technical University of Munich, Germany*
[4] *Mechanical Power Engineering Department, Faculty of Engineering EL-Mattaria, Helwan University, P.O. Box: 11718, Cairo, Egypt*
[5] *Mechanical Engineering Dept., College of Engineering and Islamic Architecture, Umm Al-Qura University, P.O. 5555, Makkah, Saudi Arabia*

†*Corresponding Author Email: mhmohamed@uqu.edu.sa*

ABSTRACT

This study examines the aerodynamics of a wing-in-ground (WIG) airfoil subjected to heaving (plunging) & pitching motion, specifically examining the distinctions in flow between transitional and turbulent states, which are essential for assessing its aerodynamic efficiency. The numerical investigation employs a validated Large Eddy Simulation (LES) model to evaluate WIG aerodynamics for a symmetrical airfoil. By analyzing variables such as pitching angle, phase shift angle, and pitching-to-heaving (PTH) ratios, the study explores their effects on thrust, lift, and drag. Findings indicate that adjusting critical heaving & pitching parameters significantly improves aerodynamic performance in turbulent flow, with thrust increasing 4 to 10-fold compared to transitional flow. Greater thrust and lift were observed in proximity to the ground. Modifying the phase-shift angle, pitching angle, and PTH led to thrust improvements of 64.9%, 2.9 times, and 4 times, respectively. The enhanced aerodynamic properties near the ground are attributed to improved flow consistency and decreased separation during heaving & pitching in turbulent flow.

Article History

Received March 9, 2025
Revised June 7, 2025
Accepted June 10, 2025
Available online September 3, 2025

Keywords:

Ground effect
Large eddy simulation
Aerodynamics
Pitching airfoil
Vortex shedding
Computational fluid dynamics

1. INTRODUCTION

Many scientists have long been intrigued by the heaving & pitching motion of airfoils, as it closely mimics the actual movement of flapping wings in real-world applications (Bryant et al., 2013; Poirel & Mendes, 2014; Barnes & Visbal, 2016; Boudis et al., 2019; Senturk & Smits, 2019). Despite the individual importance of wings in ground effect and oscillating wings, their combined study has received limited attention (Molina et al., 2011; Lu et al., 2014; Molina et al., 2016; Lee & Lin, 2022). The Wing in Ground (WIG) effect relates to the aerodynamic principles governing wings near the ground, particularly evident in racing car applications where the ground moves at freestream flow velocity. While general aerodynamic understanding exists in this field, increased resources have made dynamic testing, both experimental and numerical, more appealing (Molina et al., 2011; Lu et al., 2014; Molina et al., 2016; Adhikari et al., 2020; Sarbandi et al., 2020; Jacuzzi & Granlund, 2020; Zhi et al., 2022; Abdizadeh et al., 2022; Lee & Lin, 2022; William et al., 2024). Ground effect occurs when a lift-generating surface is within one wing-chord distance or less from the ground or water, resulting in increased lift and reduced drag. This phenomenon is caused by the ground obstructing the expansion of wing-tip vortices, which typically modify airflow around a wing and reduce lift efficiency. When impeded by the ground, these vortices significantly reduce drag and enhance lift, similar to increasing effective angles of attack (Molina et al., 2011, 2016; William et al., 2024). Flying close to the ground not only blocks vortex expansion but also increases pressure on the lower wing surface and the ground due to air compression between the airfoil and the ground (William et al., 2024). Extensive research has been conducted on the ground's impact on the aerodynamic performance of stationary inverted airfoils (Dominy, 1992; Zerihan & Zhang, 2000; Zhang & Zerihan, 2003). However, most studies have focused on fixed wings, with limited research published on flapping wings and ground effect (Molina et al., 2011; Lu et al., 2014; Molina et al., 2016; Adhikari et al., 2020; Jacuzzi & Granlund, 2020; Sarbandi et al., 2020; Zhi et al., 2022;

Nomenclature

C_D	drag force coefficient	*A/c*	heaving amplitude to chord ratio
C_T	thrust force coefficient	*A*	angle of attack
C_L	lift force coefficient	*Φ*	pitching angle
C_P	pressure coefficient	*Ψ*	phase shift angle
St_h	Strouhal number	*F*	heaving-pitching frequency
h/c	height to chord ratio	*N*	kinematic viscosity

Abdizadeh et al., 2022; Lee & Lin, 2022; William et al., 2024). Recent investigations have demonstrated that rough ground surfaces significantly influence airfoil aerodynamics and near-wall flow behaviour (Prakash Babu et al., 2025). In simulations of wing-in-ground (WIG) effect, the heaving motion of the wing is governed by a numerically implemented simple harmonic function, typically in the form of sine or cosine waves. Key parameters including amplitude (A/c), wavelength (λ/c), and wave frequency (f) are specified and adjusted as part of the simulation setup.

Researchers drew inspiration from the flight patterns of birds and insects to examine the oscillating motion of an airfoil and the flight of micro-air vehicles (MAVs) at low Reynolds number (Shyy, 2005; Shyy et al., 2007; Abate et al., 2008). The pitching and heaving movements of wings are also relevant in high Reynolds number applications, such as helicopter blades (LIIVA, 1969) and (Leishman, 2006) and wind turbines (Bertagnolio *et al.*, 2005). Lu et al. (2014) performed experimental investigations on an elliptic airfoil subjected to simple harmonic translational and rotational motions, using a flapping mechanism in conjunction with a Digital Particle Image Velocimetry (DPIV) system under fixed ground boundary conditions. However, their laminar flow experiments lacked sufficient validation. The study found that for oscillating airfoils, as the ground clearance ratio (h/c) decreased, the cycle-averaged lift (C_L) and drag (C_D) improved.

Bleischwitz et al. (2016) conducted wind tunnel investigations involving both rigid and flexible membrane wings, carrying out steady-state and transient tests over a flat moving ground surface. Their results showed that membrane wings featuring static camber and dynamic motion benefited from improved lift (C_L) when operating close to the ground. In a related work, the same authors assessed the impact of ground proximity on aerodynamic lift characteristics for both wing types across a range of AoAs (α) and relative heights (h/c), finding that both configurations delivered superior lift near the surface. Expanding on this, Bleischwitz et al. (2017) further analyzed the influence of varying α and h/c on aerodynamic behaviour, capturing oscillations in force and moment coefficients along with the membrane-induced flows. In the presence of ground effect (GE), rigid membrane configurations demonstrated enhanced lift and drag performance. A theoretical framework for incompressible aeroelasticity was introduced by Dessi et al. (2013), focusing on oscillating airfoils, and reported that proximity to the ground increased damping of oscillations. They also noted that using an inviscid assumption led to inaccuracies in capturing transient flow behaviour. Gülçat (2013) formulated a model for lift and propulsion as per vortex sheet theory and its reflection from the ground, showing that at a constant height-to-chord ratio (h/c), flapping airfoils generate significantly higher thrust than their static counterparts. Liang et al. (2014) investigated plunging airfoils above a rigid flat surface and progressing water waves, using the Discrete Vortex Method (DVM) to analyze three different oscillation types. The experimental setup encompassed heaving on a solid surface, periodic movements over water waves, and self-induced oscillations above water waves. In cases where airfoils experienced externally driven oscillations, an increase in heaving frequency led to higher time-averaged lift (C_L) and greater amplitude in lift fluctuations. For self-induced oscillatory motion, both the relative height above the surface (h/c) and the amplitude of wave (A/c) were found to influence the lift (C_L) and vertical displacement, primarily due to the airfoil's interaction with approaching wave disturbances.

Molina et al. (2011) utilized the Spalart-Allmaras model to examine the transient aerodynamic behaviour of an inverted airfoil. Their results demonstrated that operating close to the ground intensified negative lift (C_L) and decreased drag (C_D), with stall behaviour occurring near the surface. Additionally, high-frequency cases revealed forced vortex shedding at the trailing edge. Wu and Zhao (2013) numerically analyzed ground effect on a flapping NACA0012 airfoil using the Immersed Boundary-Lattice Boltzmann Method. A fixed ground plane was modeled while systematically varying the height ratio (h/c) and oscillation frequency. The study found that reducing h/c and increasing frequency promoted higher thrust and lift forces. In a separate investigation, Molina et al. (2016) conducted simulations combining heaving and pitching motions in ground effect using the Spalart-Allmaras model. However, the study's validation approach was limited, as it involved comparisons between viscous results and analytical inviscid solutions, and lacked details such as the Courant number, which raised concerns about result reliability. Ito and Iwashita (2016) carried out both computational and experimental studies on unsteady WIG motion involving heaving kinematics. Their numerical approach used a 3D inviscid Boundary Element Method (BEM) to model flapping motion above a rigid ground, while parallel experiments were conducted with a 3D wing oscillating over a dry water surface in a towing tank. They reported that drag (C_D) exhibited pronounced nonlinear variations under heaving motion, which became more significant with rising amplitude (A/c) and decreasing ground clearance (h/c). Overall, unsteady aerodynamic effects were found to intensify at lower h/c values or higher heaving frequencies.

In addition to unsteady aerodynamic behaviour, the stability of aerodynamic geometries such as flapping airfoils and WIG craft is of significant concern. Prior studies have examined flow instabilities and wake behaviour in these contexts. For instance, Türkyılmazoglu et al. (1999) analyzed the absolute instability of thin wakes in incompressible and compressible fluids, providing foundational insights into wake behaviour relevant to airfoil oscillations. Turkyilmazoglu (2002) investigated flow near the trailing edge of Joukowski-type profiles, highlighting local separation, vortex dynamics, and the evolution of small disturbances into globally unstable modes that affect airfoil stability. These theoretical works offer critical context to complement numerical and experimental analyses of WIG aerodynamics, particularly regarding flow stability and vortex shedding.

2. PREVIOUS WORK GAP AND NOVELTY

This study evaluates the wing-in-ground (WIG) aerodynamics of a symmetrical airfoil by considering the influence of combined heaving and pitching motion. Although previous investigations have addressed this topic (Molina et al., 2011; Lu et al., 2014; Molina et al., 2016; Adhikari et al., 2020; Sarbandi et al., 2020; Jacuzzi & Granlund, 2020; Zhi et al., 2022; Abdizadeh et al., 2022; Lee & Lin, 2022; William et al., 2024), few have explored the impact of heaving-pitching motion near ground regions in both transitional and turbulent flow conditions. Current research typically examines WIG aerodynamics at either high or low Reynolds numbers (Molina et al., 2016; Adhikari et al., 2020; Sarbandi et al., 2020; Lee & Lin, 2022). This study aims to bridge this knowledge gap by conducting a more comprehensive validation. It then analyzes the WIG combined with heaving-pitching motion in transitional (low Reynolds number) and turbulent (high Reynolds number) flow regimes. The research encompasses a broader range of variables and incorporates frequency-domain analysis. Additionally, Turbulent flow simulations are performed with Large Eddy Simulation (LES) rather than the Unsteady Reynolds-Averaged Navier-Stokes (URANS) approach. As the standard OpenFOAM library does not natively support simultaneous heaving and pitching motions, a custom solver was developed to enable combined heaving-pitching simulations. This newly implemented tool is capable of handling such motions both in and out of ground effect conditions, with the added flexibility of tuning the frequency ratio between the heaving and pitching components. Although the simulations were carried out using dimensional inputs in OpenFOAM, the key flow parameters and results are reported in non-dimensional form (e.g., h/c, A/c, Strouhal number) to ensure generality and to facilitate meaningful comparison with other studies in the fluid dynamics literature.

3. CFD Simulation Methodology

This study investigated a fluid flow that is two-dimensional, transient, and incompressible. The fluid under examination was Newtonian and characterized by a constant dynamic viscosity (μ) and density (ρ). The study utilized numerical methods based on discretized continuity equation and momentum equation to analyze the relevant flow characteristics. The governing equations used in this study include the continuity equation and the incompressible Navier–Stokes momentum equations in two dimensions, which form the foundation of most CFD simulations (Versteeg and Malalasekera, 2007). The analysis incorporates versions of the continuity and Navier-Stokes equations in its formulation:

$$\left(\frac{\partial u}{\partial x}+\frac{\partial v}{\partial y}\right)=0 \tag{1}$$

$$\rho\left(\frac{\partial u}{\partial t}+u\frac{\partial u}{\partial x}+v\frac{\partial u}{\partial y}\right)=-\frac{\partial p}{\partial x}+\mu\left(\frac{\partial^2 u}{\partial x^2}+\frac{\partial^2 u}{\partial y^2}\right)+S_{b,x} \tag{2}$$

$$\rho\left(\frac{\partial v}{\partial t}+u\frac{\partial v}{\partial x}+v\frac{\partial v}{\partial y}\right)=-\frac{\partial p}{\partial y}+\mu\left(\frac{\partial^2 v}{\partial x^2}+\frac{\partial^2 v}{\partial y^2}\right)+S_{b,y} \tag{3}$$

where $S_{b,x}$, and $S_{b,y}$ denote the body forces acting along the x, and y directions.

A range of numerical techniques is available for solving the governing flow equations, such as Direct Numerical Simulation (DNS), Large Eddy Simulation (LES), and the Unsteady Reynolds-Averaged Navier–Stokes (URANS) framework. Among these, the WALE (Wall-Adapting Local Eddy-viscosity) LES model is commonly favored for accurately capturing wall-bounded flow behaviour. Simulations of WIG-craft flow focus on examining the airflow between a dynamic ground surface often used to represent water beneath a flying vehicle and a fixed airfoil, making them well-suited for application of the WALE LES model. This turbulence model is particularly effective in resolving near-wall flow behaviour, including accurate estimation of wall shear stress. Precise shear stress predictions enable more reliable calculations of skin friction drag components. Additionally, WALE LES effectively reproduces large eddies generated downstream. The WALE model excels at predicting wall asymptotic behaviour in flows confined by walls (Ben-Nasr et al., 2017)As described by Nicoud and Ducros (1999), the subgrid-scale viscosity in the WALE LES model is defined through the following formulation:

$$\nu_{sgs}=C_k\,\Delta\sqrt{k_{sgs}} \tag{4}$$

where C_k denotes a model constant ($C_k=0.094$) and k_{sgs} represents the kinetic energy associated with the subgrid scale.

Few manipulations resulted in this eddy viscosity expression:

$$\nu_{sgs}=(C_w\,\Delta)^2\,\frac{\left(s_{ij}^d s_{ij}^d\right)^{3/2}}{\left(\bar{\varepsilon}_{ij}\bar{\varepsilon}_{ij}\right)^{5/2}+\left(s_{ij}^d s_{ij}^d\right)^{5/4}} \tag{5}$$

where $\bar{\varepsilon}_{ij}$ denotes the strain rate tensor at the resolved-scale, S_{ij}^d corresponds to the squared magnitude of the symmetric, traceless part of the velocity gradient tensor,

Table 1 Summary of Boundary Conditions Used in the CFD Simulations

Boundary	Type	Condition Applied
Inlet	Velocity Inlet	Uniform velocity with turbulence intensity of 0.1%
Outlet	Pressure Outlet	Zero-gauge pressure
Moving Road	Moving Wall	Matches freestream inlet velocity to simulate moving ground effect
Airfoil	No Slip	Heaving–pitching motion applied using moving wall velocity
Symmetry Top	Symmetry	No normal flow or shear (symmetry condition)
Side Boundaries	Symmetry	Symmetric in spanwise direction (2D)

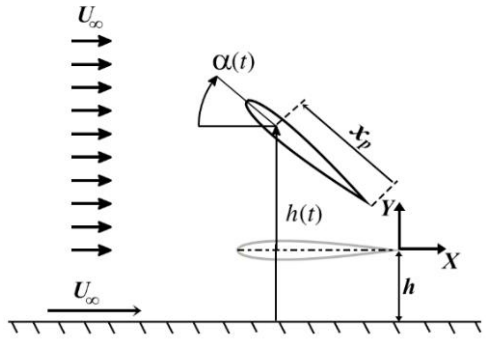

Fig. 1 Coordinate system and reference parameters associated with the heaving-pitching motion in WIG configurations

and C_w is a model constant ($C_w = 0.325$).

The reference parameters and coordinate axes related to the combined plunging & pitching motion in the WIG configuration are shown in Fig. 1. Figure 2 illustrates the simulation domain used to model the heaving & pitching motion combined in WIG conditions, as presented by Lehmkuhl Barba et al. (2011). The boundary conditions used in the study are illustrated under Table 1. A symmetric boundary condition was implemented along the spanwise axis. Geometric parameters were non-dimensionalized using the chord length (c) as the reference scale. The computational grid was automatically extended by 1.131c in the direction normal to the surface, and a no-slip condition was applied along the wall boundary. A turbulence intensity of 0.1% was set for the velocity inlet, BC. The pressure outlet was assumed to have a constant static pressure. The air kinematic viscosity (ν) was established as 1.50575×10^{-5} m^2/s. As a moving wall boundary, the bottom BC is configured to match the inlet air velocity (Barber et al., 1999). In simulations of transitional flow, a Reynolds number of $Re = 2.5\times10^4$ was applied for the inlet conditions. In turbulent flow studies related to WIG, the Reynolds number was set to 8×10^5, following Moore et al. (2002). The wing wall boundary condition is assigned a "movingWallVelocity" to enable its movement during simulations.

The Navier-Stokes equations were resolved using OpenFOAM (Weller *et al.*, 1998), which utilizes the WALE LES turbulence model and the solver employed is "pimpleDyMFoam". To maintain a Courant number of 0.5, a variable time step was implemented. The computational domain was divided into 32 partitions by using the scotch algorithm for parallel processing in OpenFOAM. Each case required approximately 2200 core hours of processing time. The governing equations were discretized using second-order accurate numerical schemes. Suitable and stable solvers were chosen for handling pressure fields and turbulence-related variables. To facilitate mesh motion and deformation, the "displacementLaplacian" method was utilized. A customized OpenFOAM solver named "twoDOForiginal" was developed specifically to implement wing's the heaving-pitching motion. The airfoil's motion was prescribed based on the following heaving & pitching definitions:

$$h(t) = h + A * sin(2\pi ft + \Psi) \quad (6)$$

$$\alpha(t) = \alpha + \Phi * sin(2\pi ft) \quad (7)$$

where (h) denotes the altitude of flight in meters, (A) represents the magnitude of heaving in meters, (f) denotes the motion frequency in Hertz, (Ψ) refers to the angular difference between heaving and pitching movements in degrees, (α) indicates the starting angle of attack (AoA) in degrees, and (Φ) expresses the extent of pitching in degrees. Sinusoidal functions, represented by equations (6) and (7), were used to define the airfoil's heaving and pitching motions, characterizing its vertical and angular displacements as functions of time. This formulation allows precise control over key motion parameters, including amplitude, frequency, phase shift, and initial angle of attack. Following the methodology of Moriche et al. (2017), who successfully employed a similar model to study unsteady aerodynamic forces at low Reynolds numbers, this approach ensures accurate reproduction of transient flow behaviour. This formulation is adopted as it provides the most complete and validated representation of heaving & pitching motion, making it ideal for capturing complex interactions between the airfoil and surrounding flow. Positioned at a point X_p measured from the trailing edge, the pitching axis corresponded to 75% of the chord length.

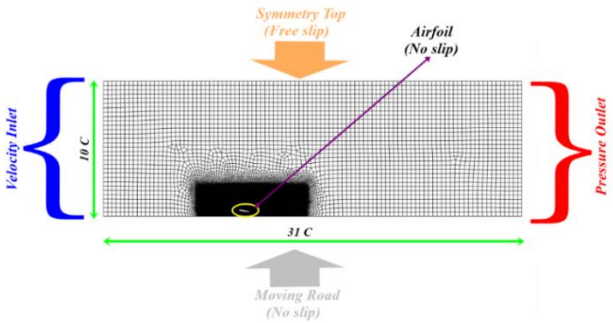

Fig. 2 Principal dimensions and boundary conditions of the computational domain for the WIG configuration

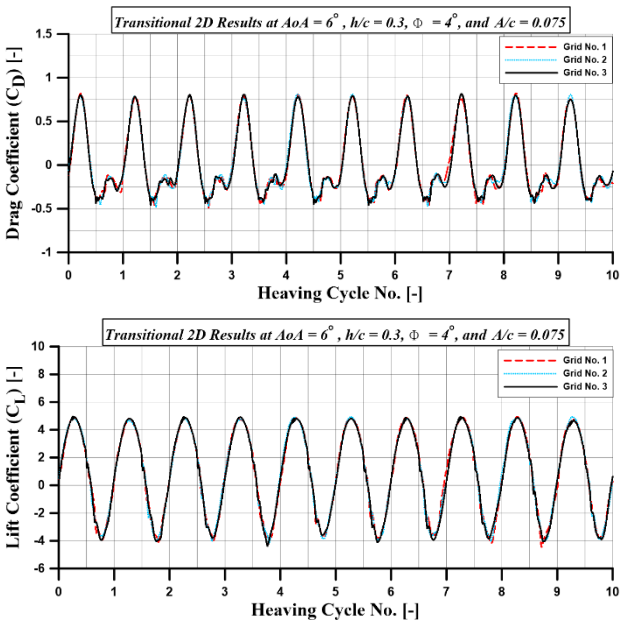

Fig. 3 Comparison of force coefficient variations across multiple mesh resolutions for heaving-pitching WIG configurations (Transitional flow)

In parametric analyses, it is beneficial to express length-related variables in a non-dimensional form, particularly as (h/c) and (A/c). According to Wu and Zhao (2013), the Strouhal number (Sth) for a heaving airfoil is defined as follows:

$$St_h = \frac{2A\,f}{U_\infty} \tag{8}$$

In this equation, (A) represents the heaving amplitude in meters, (f) denotes the oscillating frequency in Hertz, and (U∞) signifies the free-stream velocity in meters per second. The investigation focused on a Strouhal number (St_h) range of 0.1 to 0.2 in both transitional flow and turbulent flow. Wu and Zhao (2013) previously investigated this Strouhal number (S_{th}) range for the case of pure heaving motion in ground effect. For the transitional WIG plunging & pitching scenario in the present study, the adopted reference parameters include: h/c = 0.3, A/c = 0.075, frequency f = 3.746 Hz, phase angle Ψ = 0°, angle of attack α = 6°, and pitching amplitude Φ = 4°. These conditions were maintained for the turbulent case, with the exception of frequency, which was modified to 119.87 Hz to preserve a fixed Strouhal number. Freestream velocity (U∞) was specified as 1.1875 m/s for transitional simulations and 38 m/s for turbulent flow. A chord length (c) of 0.317 m and a reference Strouhal number of 0.15 were used for the standard heaving-pitching configuration. The transitional flow near the ground was analyzed for a wing executing combined heaving and pitching motions at a Reynolds number of 2.5×10^4 over a 16.55 s simulation. For the turbulent regime, simulations were carried out at Re = 8×10^5 for a total duration of 0.5172 s. In each scenario, the simulation duration was long enough to capture at least 40 full cycles of the heaving-pitching motion. To ensure numerical reliability, a mesh independence study was conducted using LES simulations for NACA0012 airfoil under the specified reference conditions. The mesh resolution varied from 211,064 cells in Grid (1) to 274,816 cells in Grid (3). Outcomes of the transitional flow and turbulent flow are illustrated in Figs. 3 and 4, respectively. Grid independence was evaluated based on the average C_L and C_D computed over the first and second halves of the simulation cycles, as presented in Tables 2 and 3. As variations between grid (2) and grid (3) remained within 5%, grid (2) was selected for subsequent simulations to balance accuracy and efficiency. Figure 5 illustrates the details of the employed grid structure, featuring finer grid cells in the downstream direction behind the wing to capture the vortex structure effectively. The periodic trends observed in Figs. 3 and 4 are a direct result of the sinusoidal heaving-pitching motion prescribed in equations (6) – (7). This behaviour is physically realistic and aligns with theoretical expectations for harmonic airfoil motion, where periodic forcing naturally leads to periodic aerodynamic responses.

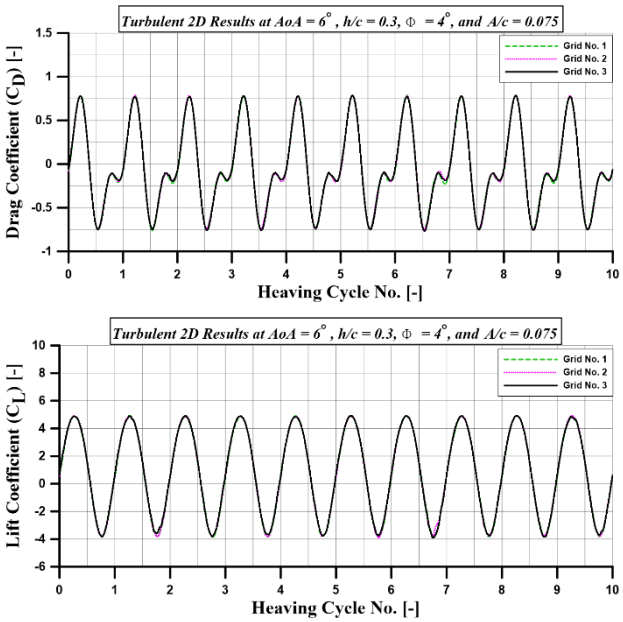

Fig. 4 Comparison of force coefficient variations across multiple mesh resolutions for heaving-pitching WIG configurations (Turbulent flow)

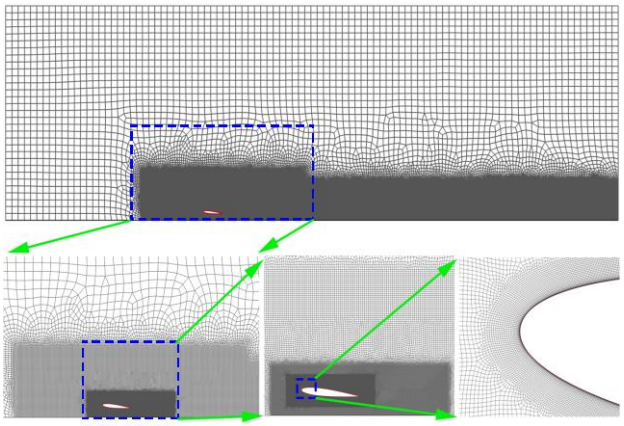

Fig. 5 Grid structure for the present investigation (grid2)

Table 2 Grid Independence Study – Transitional Flow

Force Coefficient	Grid 1	Grid 2	Grid 3	% Diff 1→2	% Diff 2→3
C_D (1st Half)	0.311	0.346	0.357	15.0%	3.1%
C_D (2nd Half)	–0.292	–0.265	–0.254	8.6%	4.1%
C_L (1st Half)	2.88	3.20	3.066	9.5%	4.1%
C_L (2nd Half)	–1.55	–1.409	–1.343	27.2%	4.6%

Table 3 Grid Independence Study – Turbulent Flow

Force Coefficient	Grid 1	Grid 2	Grid 3	% Diff 1→2	% Diff 2→3
C_D (1st Half)	0.294	0.327	0.315	10.1%	3.6%
C_D (2nd Half)	–0.389	–0.354	–0.344	9.8%	2.8%
C_L (1st Half)	2.562	2.847	2.782	10.0%	2.2%
C_L (2nd Half)	–1.898	–1.725	–1.658	10.0%	3.8%

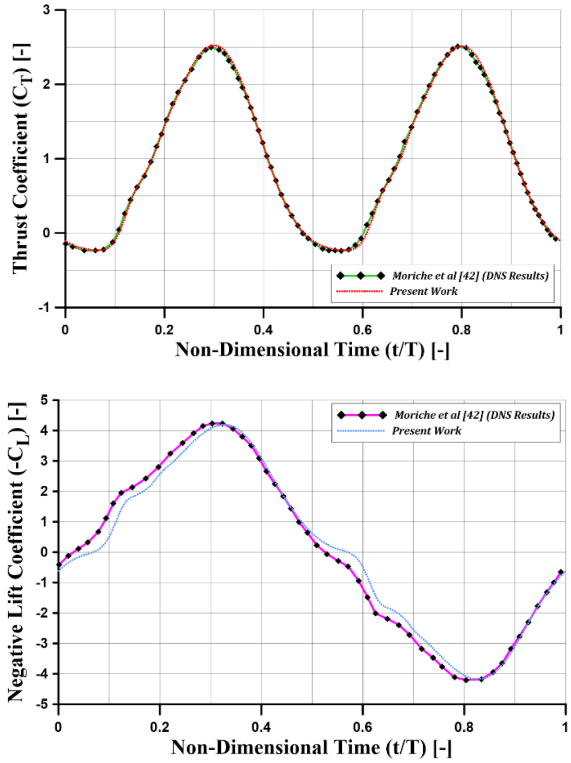

Fig. 6 Comparison between simulation results from the developed heaving-pitching model and DNS data published by Moriche et al. (2017)

3.1 Simulation Validation for Airfoil Undergoing Heaving-Pitching Motion

The newly developed heaving-pitching solver for OpenFOAM was validated against the Direct Numerical Simulation (DNS) results provided by Moriche et al. (2017). To replicate the wing's heaving-pitching behaviour in free-flight conditions, equivalent boundary conditions were implemented. The validation utilized the following parameters: Reynolds number Re = 1000, amplitude ratio A/c = 1, phase shift Ψ = 270°, angle of attack α = 0°, pitching amplitude Φ = 30°, and a lowered frequency k = [2πfc/U∞] = 1.41, corresponding to case (A090) from their study. As illustrated in Fig. 6, the computed C_T and C_L coefficients from the present solver closely align with those reported by Moriche et al. (2017), confirming the accuracy of the method. Following successful validation, the investigation proceeded to examine wing motion in proximity to the ground.

4. Results and Discussion

In all cases, the Reynolds number for transitional flow was maintained at 2.5×10^4, while for turbulent flow, it remained constant at 8×10^5. The key parameters for the heaving-pitching motion were maintained at their reference values: a pitching angle (Φ) of 4°, phase shift angle (Ψ) of 0°, and Strouhal number (St_h) of 0.15. The heaving-pitching frequencies (f) used were 3.746 Hz for the transitional flow and 119.87 Hz for the turbulent flow. These conditions were consistent across all scenarios except for the specific parameter under investigation. This work introduces the first use of frequency analysis to evaluate unsteady aerodynamic forces, focusing on drag (C_D) and lift (C_L). The outcomes reveal that surface vortices induced by viscous effects exert only a limited influence on the overall aerodynamic performance. In turbulent flows, the pressure coefficient (C_P) patterns closely resemble those observed in transitional flows. As a result, the primary focus shifts to thrust (C_T), which shows an increase of more than tenfold compared to its value in transitional flow.

4.1 Effect of Pitching Angle (Φ)

Within the transitional flow regime, considering the pitching amplitude (Φ) as the main variable, it is noted that at Φ = 6°, The influence of the flow vortices on the shifting flat surface is insignificant, as illustrated in Fig. 7. This results in more stable and uniform oscillatory behaviour of the aerodynamic forces at elevated Φ values. Larger pitching amplitudes intensify flow separation, which in turn reduces both C_L and C_D. Figure 8 presents the distribution of the pressure coefficient (C_P) over the surface of the airfoil. At the phase t/T = 0.25, increasing Φ leads to a stronger suction effect (more negative C_P) on the upper surface within the initial 20% of the chord. Conversely, on the lower surface, C_P values decrease significantly from x/c = 0 to 0.8, exceeding the upper surface gains and ultimately resulting in reduced C_L and increased form drag (C_D) due to diminished wake pressure. At t/T = 0.75, higher amplitudes of pitching continue to reduce the magnitude of lower surface negative pressure ($-C_P$) over the same chord range, suggesting

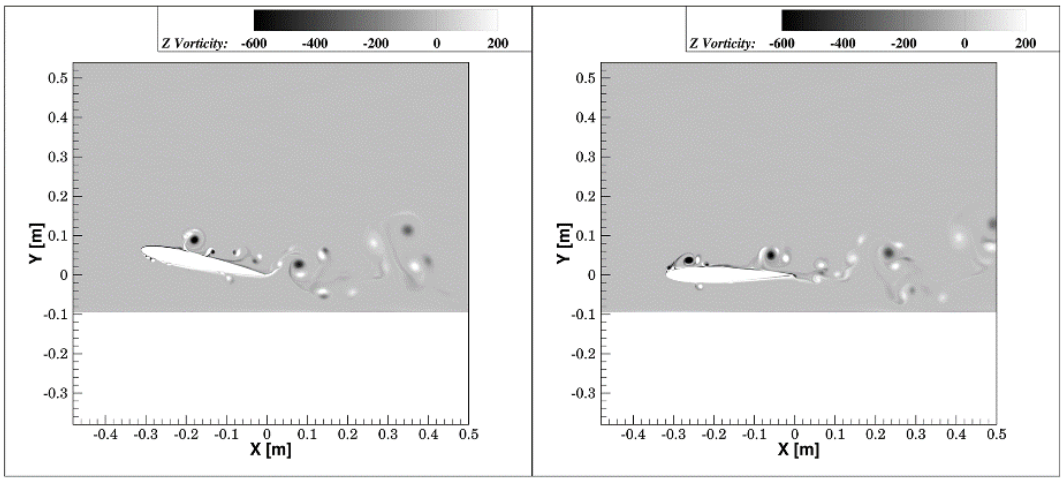

t/T = 0.25 *t/T* = 0.75

Φ= 6º

Fig. 7 Influence of the ground on the airflow around a plunging & pitching wing with a pitching amplitude of Φ = 6° [Transitional flow]

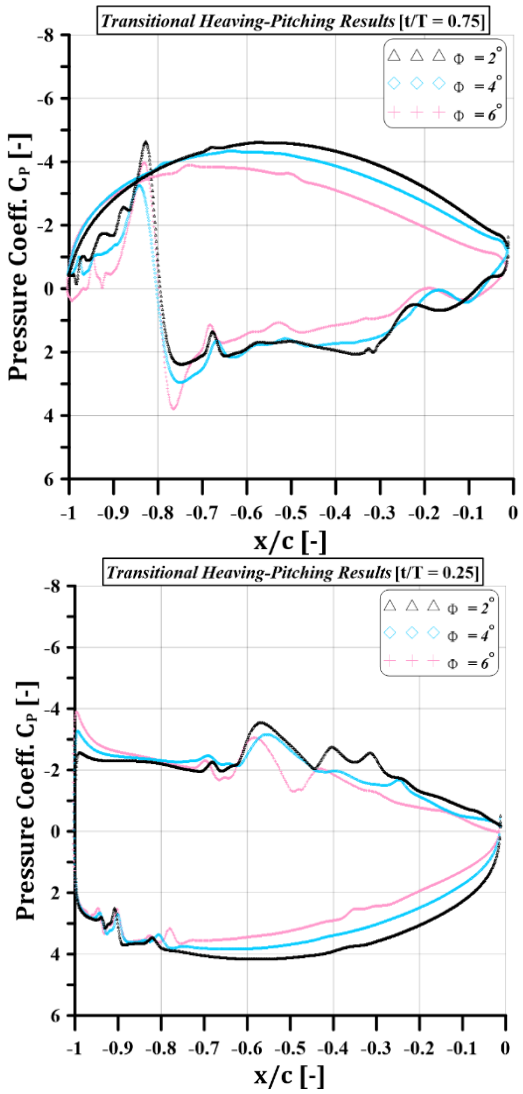

Fig. 8 Pressure coefficient (C_P) distribution over wing surface for two stages of plunging & pitching cycle at different pitching angle (Φ) [Transitional flow]

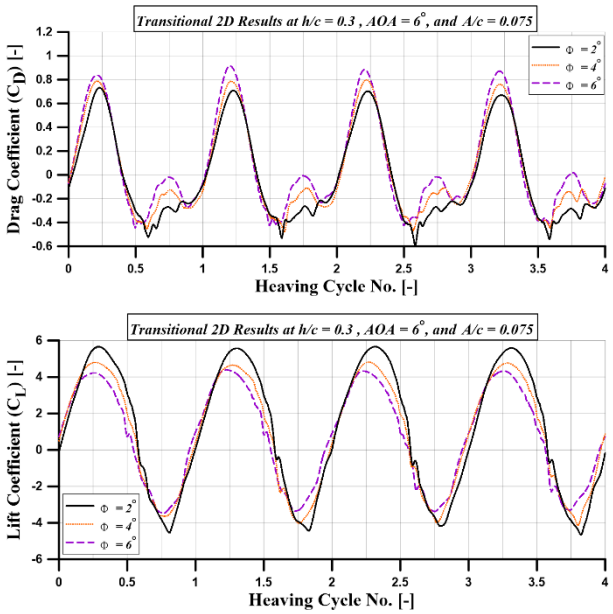

Fig. 9 Changes in aerodynamic forces for a wing-in-ground (WIG) configuration undergoing plunging & pitching motion at different pitching amplitudes (Φ) in transitional flow

a trend toward lower negative lift ($-C_L$) with surging Φ. As depicted in Fig. 9, the trends in aerodynamic force coefficients correspond with the pressure field behaviour. While C_L fluctuations tend to reduce with greater Φ, C_D oscillations between t/T = 0 and 0.5 become more pronounced. Additionally, the thrust coefficient (C_T) over the latter half of the oscillation cycle declines with increasing Φ. Nonetheless, the aerodynamic coefficients display improved cycle-to-cycle consistency at higher pitching amplitudes.

Figure 10 displays the amplitude spectra of C_L and drag C_D associated with the primary frequency of plunging & pitching and its higher-order harmonics. At a pitching

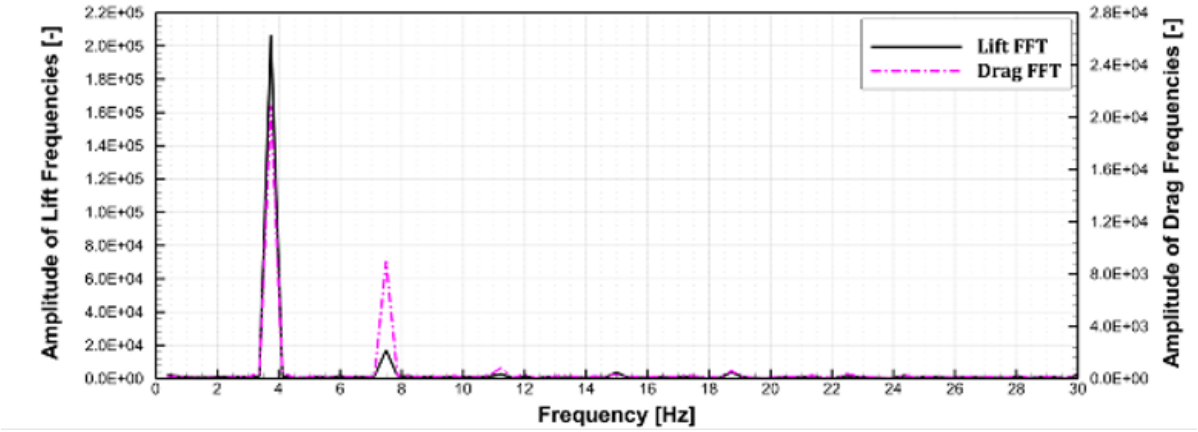

(a) $\Phi=2^{\circ}$

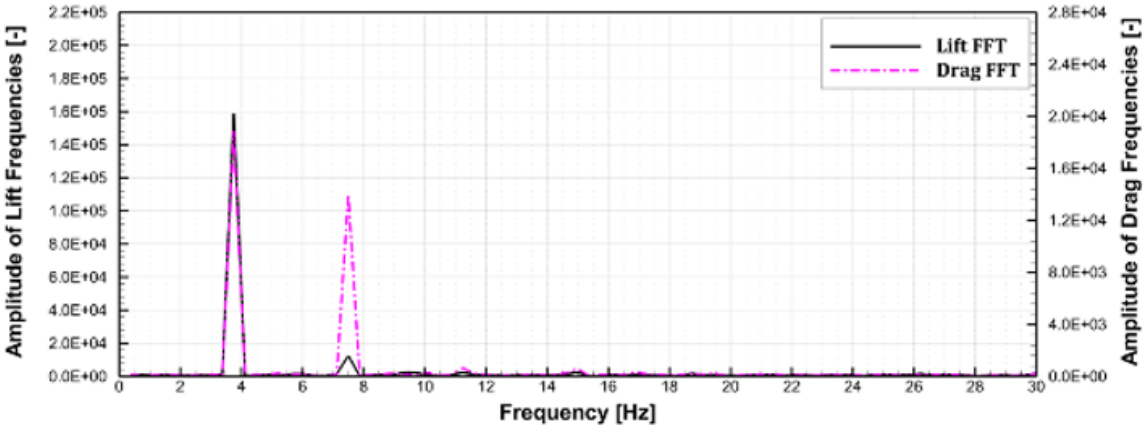

(b) $\Phi=6^{\circ}$

Fig. 10 Frequency analysis of lift and drag variations for a plunging & pitching WIG configuration at varying pitching amplitudes (Φ) [Transitional flow]

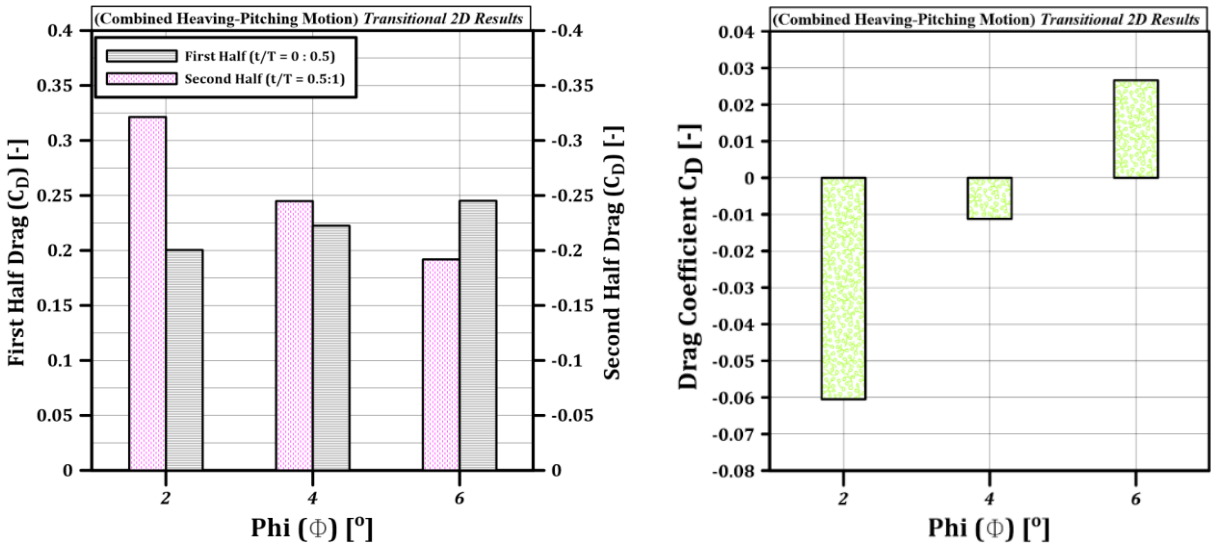

(a) (b)

Fig. 11 Mean impact of each half-cycle to drag coefficient (C_D), and (b) total cycle-averaged drag (C_D) for various pitching amplitudes (Φ) [Transitional flow]

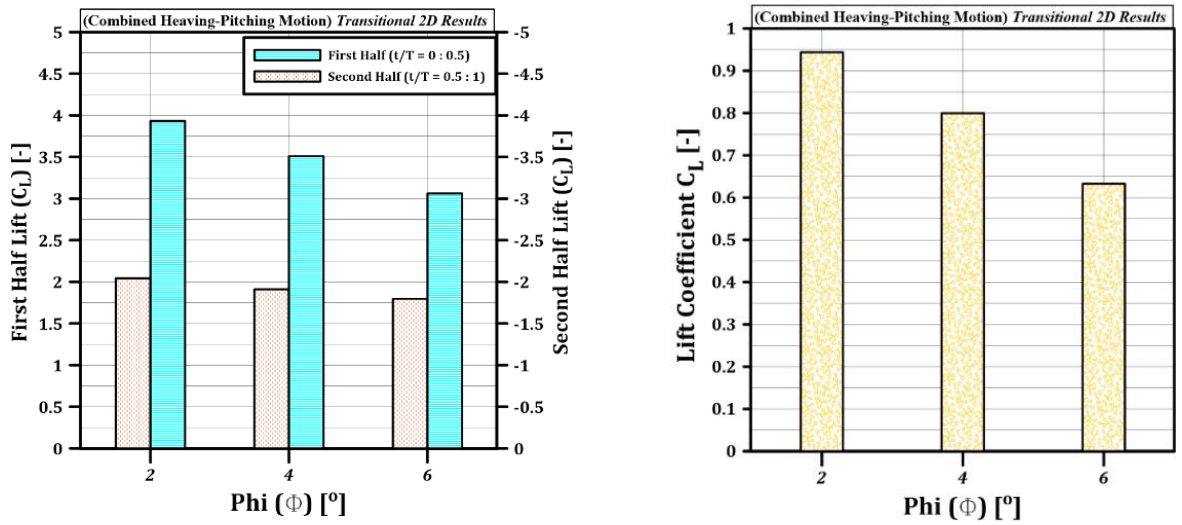

(a) (b)

Fig. 12 (a) Mean lift coefficient (C_L) contribution from each half-cycle and (b) overall cycle-averaged lift (C_L) for different pitching amplitudes (Φ) [Transitional flow]

amplitude of Φ = 2°, the lift response is primarily concentrated at the base frequency, while at Φ = 6°, the drag spectrum shows a more pronounced peak at the second harmonic (2f). Figure 11a) illustrates how every half-cycle of the plunging & pitching motion contributes to C_D. As Φ increases, both the drag and thrust (C_T) generated during every half of the oscillation diminish. Notably, at Φ = 6°, the coefficient of drag (C_D) surpasses the corresponding coefficient of thrust (C_T). Consequently, for this pitching angle (Φ), the airfoil does not generate thrust, as shown in Fig. 11 (b). In a transitional flow, the airfoil exhibited its best thrust performance per heaving-pitching cycle at Φ = 2° with a (C_T) of 0.06. As shown in Fig. 12(a), both the positive and negative lift coefficients (C_L and $-C_L$) decrease during every half-cycle as the amplitude of pitching (Φ) increases. Despite variations, the positive lift consistently exceeds the negative counterpart for all examined Φ values. As shown in Fig. 12(b), optimal C_L output for the plunging & pitching airfoil occurs at Φ = 2°. Beyond this point, mean lift per cycle shows a steady decline, with a reduction of nearly 33% observed at Φ = 6°. These findings suggest that lower pitching amplitudes are more favorable for achieving efficient thrust (C_T) and lift (C_L) generation in transitional flow conditions for WIG applications.

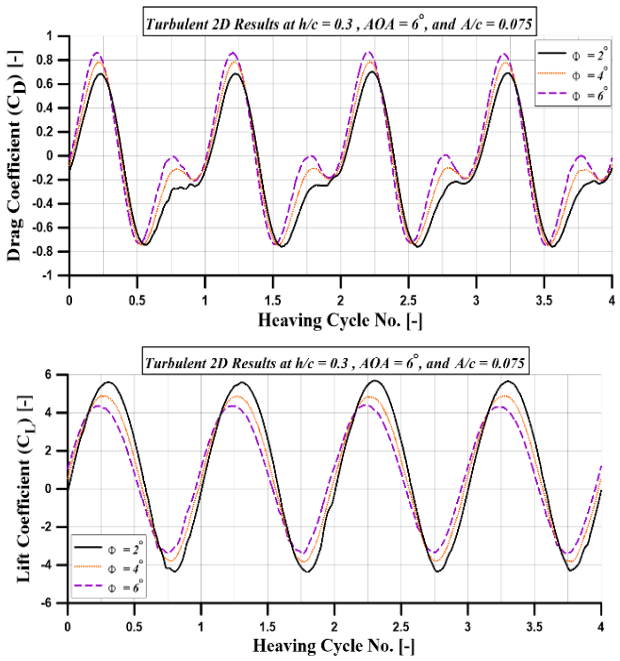

Fig. 13 Aerodynamic force trends for plunging & pitching WIG configuration at varying pitching amplitudes (Φ) [Turbulent flow]

Figure 13 Improved drag coefficient (C_D) characteristics for a heaving-pitching airfoil under turbulent flow conditions in ground proximity. Even at a pitching amplitude of Φ = 6°, the force oscillations became more uniform within each cycle, which is linked to improved flow formation around the airfoil. As depicted in Fig. 14(a), both drag (C_D) and thrust (C_T) show a gradual reduction as the pitching amplitude (Φ) increases under turbulent conditions. Interestingly, during the initial half-cycle (t/T = 0 to 0.5), the drag trend in turbulent flow contrasts with that seen in transitional flow. As Φ increases, the discrepancy between C_D and C_T gradually decreases. Figure 14(b) shows that the peak thrust (C_T) is achieved at Φ = 2°, reaching 0.175, but drops by 32.2% when Φ is raised to 6°. It is noteworthy that under transitional conditions, no thrust is generated at Φ = 6°, whereas at Φ = 2°, turbulent flow thrust is nearly 2.9 times that of transitional flow. Figures. 15(a) and 15(b) display lift (C_L) characteristics that align with the patterns observed in transitional flow, yet turbulent conditions consistently lead to greater average lift per cycle. Specifically, at Φ = 2°, turbulent flow achieves approximately 30% higher lift than transitional flow. Overall, turbulent flow provides superior aerodynamic performance in terms of both C_T and C_L for a WIG craft executing plunging & pitching motion.

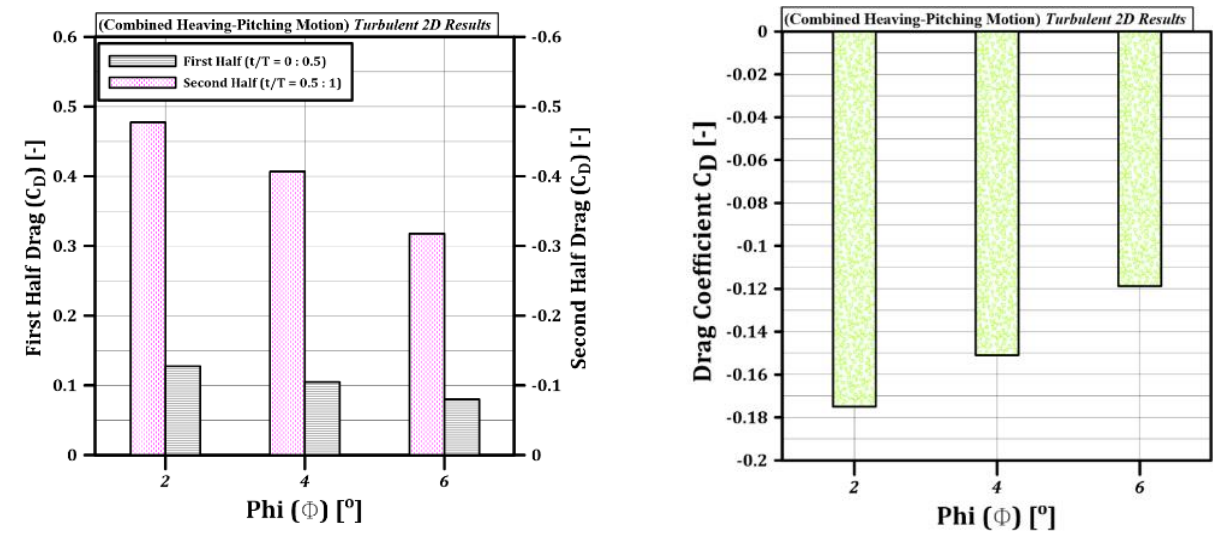

(a) (b)

Fig. 14 (a) Mean drag coefficient (C_D) contribution from each half-cycle and (b) cycle-averaged drag (C_D) at various pitching amplitudes (Φ) [Turbulent flow]

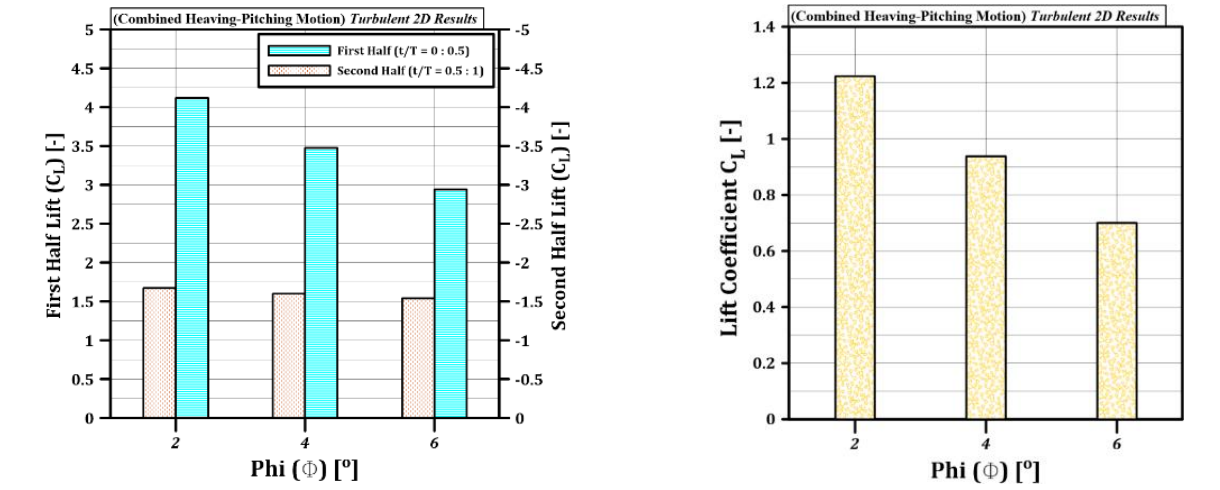

(a) (b)

Fig. 15 (a) Average lift coefficient (C_L) generated during each half-cycle and (b) total cycle-averaged lift (C_L) across different pitching amplitudes (Φ) [Turbulent flow]

4.2 Effect of Phase Shift Angle (Ψ)

This part examines two selected phase-shift angles: Ψ = 90° and Ψ = 180°. The pitching motion remained constant, whereas the heaving phase advanced. To maintain numerical stability during unsteady simulations owing to substantial grid deformations, the amplitude of heaving was reduced to A/c = 0.05. Figure 16 illustrates the vortex structures formed at a phase shift angle of Ψ = 180° under transitional conditions. The formation of larger eddies in the wake region indicates an increased pressure difference between the airfoil's upper and lower surfaces. However, despite the prominent vortex formations at this phase angle, their interaction with the ground remains limited, contributing to more consistent oscillatory behaviour in aerodynamic forces. Figure 17 shows the distributions of the pressure coefficient (C_P) over the airfoil surface at various points throughout the heaving-pitching cycle. Typically, four distinct C_P distribution profiles emerge for each value of Ψ, and three of these are illustrated based on the orientation of the airfoil during different phases. Significant differences in C_P are observed across Ψ angles. For instance, for Ψ = 90°, at t/T = 0.25, the peak suction pressure ($-C_P$) reaches −14.62, which is approximately 29.1% lower than the corresponding peak at t/T = 0.5 for Ψ = 0°. These differences reveal that varying the phase angle influences the timing and magnitude of peak pressures, thereby impacting the aerodynamic forces generated. As shown in Fig. 18, the resulting aerodynamic force coefficients reflect these phase-related effects. An increase in Ψ is associated with a rise in C_T, and at Ψ = 180°, the C_D fluctuations are nearly inverted when compared to Ψ = 0°. Across all Ψ values, the force coefficients follow a regular oscillation pattern, indicating minimal disruption from ground-induced vortex interactions. Notably, the sharp changes observed in the pressure coefficient (C_P) profiles at Ψ = 180° are physical in nature. These arise due to the phase-aligned interaction between shed vortices and the ground surface, which leads to abrupt pressure variations on the airfoil surfaces during specific phases of the cycle.

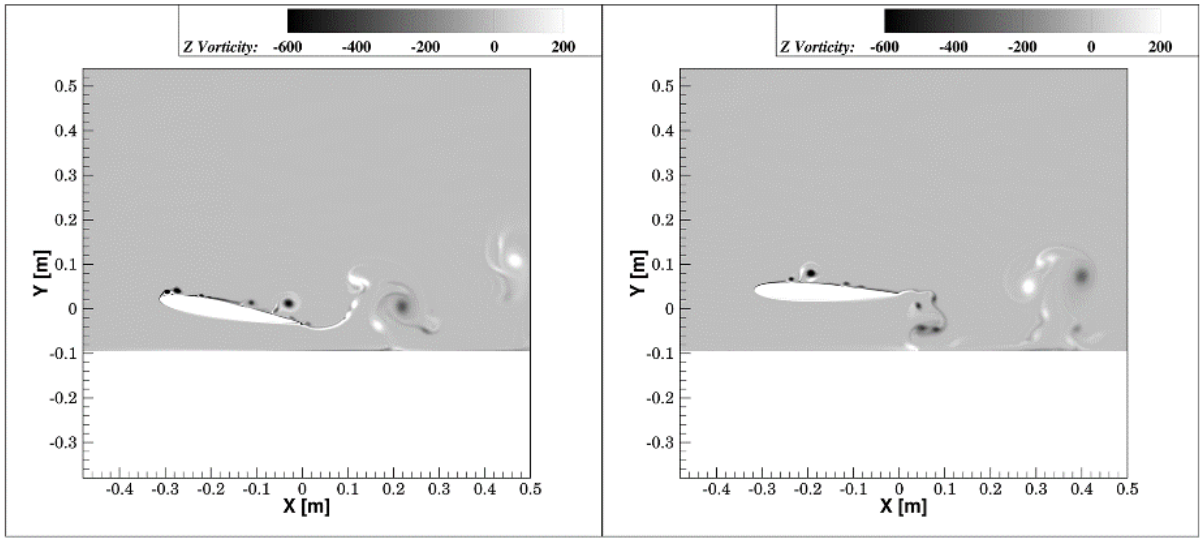

t/T = 0.25 *t/T* = 0.75

Phase Shift = 180 º

Fig. 16 Flow interaction between the ground and a plunging & pitching wing at a phase shift angle of Ψ = 180° [Transitional flow]

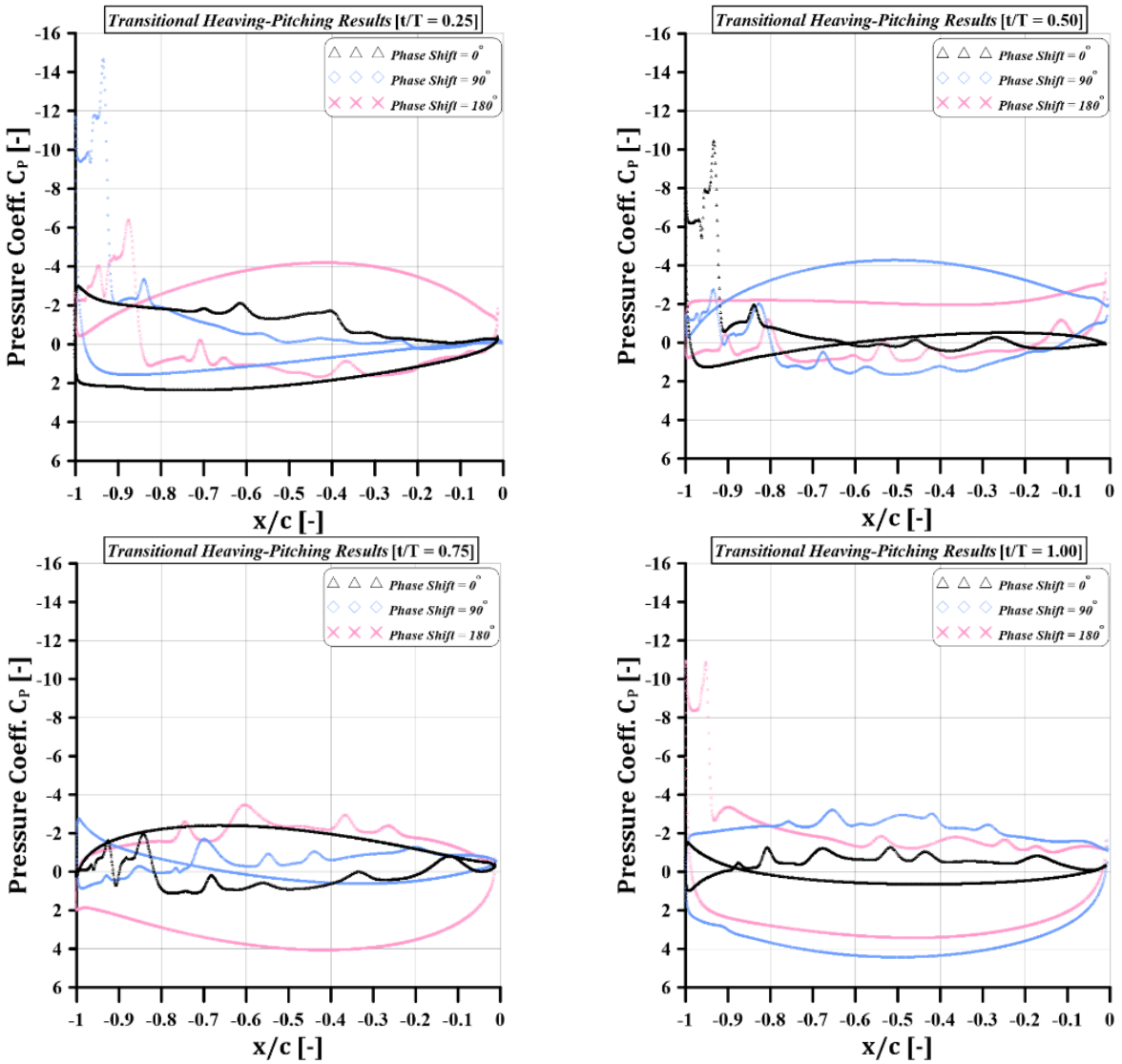

Fig. 17 Wing surface pressure coefficient (C_P) distribution across four stages of the plunging & pitching cycle for various phase shift angles (Ψ) [Transitional flow]

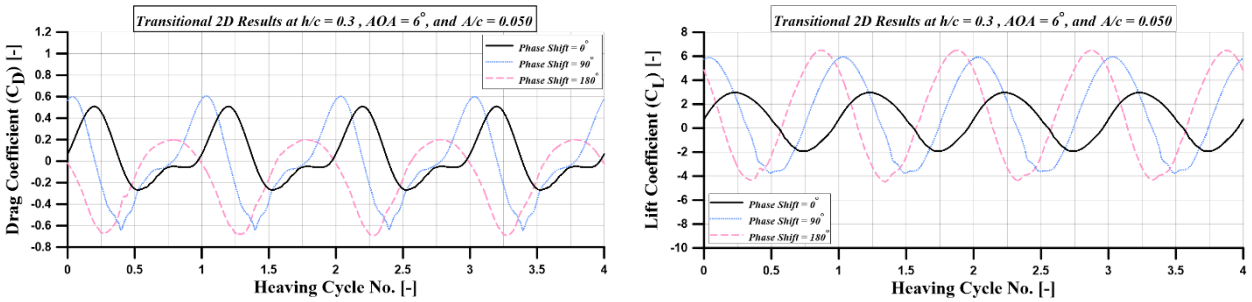

Fig. 18 Aerodynamic force variation for plunging & pitching WIG configuration at multiple phase shift angles (Ψ) [Transitional flow]

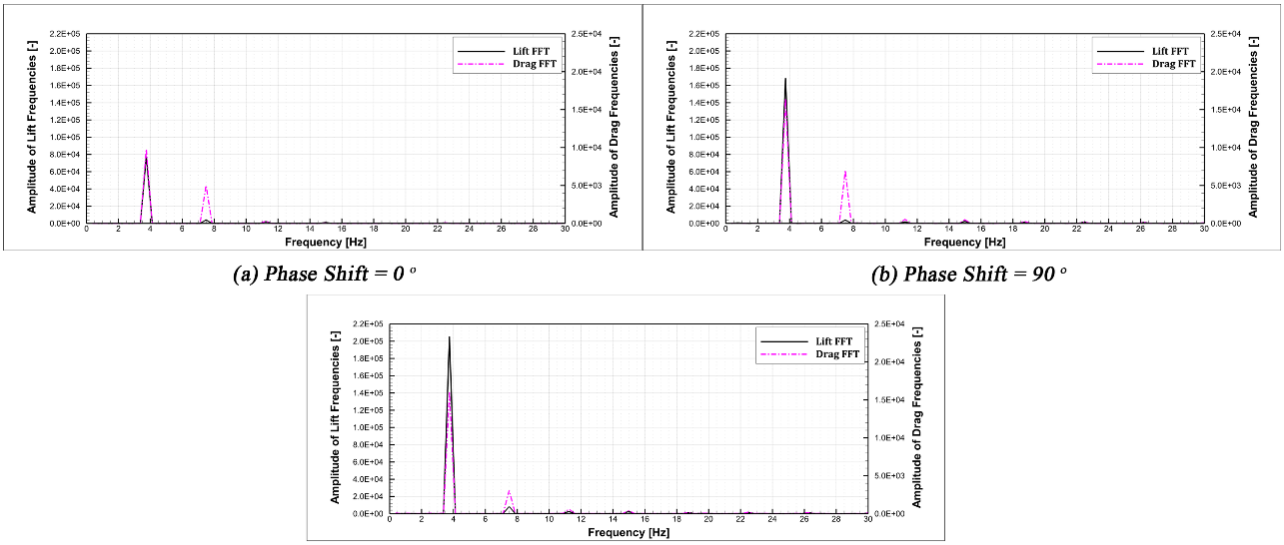

(a) Phase Shift = 0 ° *(b) Phase Shift = 90 °*

(c) Phase Shift = 180 °

Fig. 19 Frequency analysis of aerodynamic forces for plunging & pitching WIG configuration across different phase shift angles (Ψ) [Transitional flow]

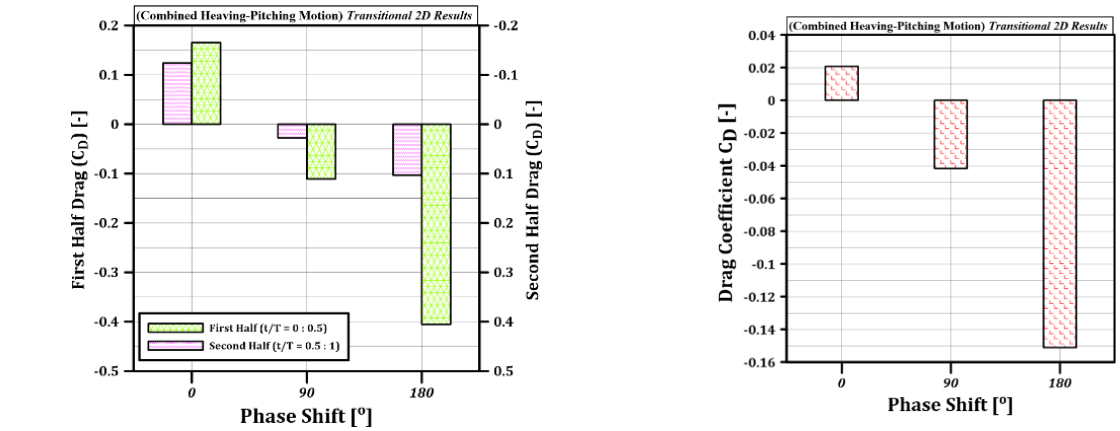

(a) (b)

Fig. 20 (a) Mean drag coefficient (C_D) contribution from each half-cycle and (b) total cycle-averaged drag (C_D) across various phase shift angles (Ψ) [Transitional flow]

Figure 19 presents the frequency components of aerodynamic forces across a range of phase-shift angles (Ψ). As Ψ increases, the primary frequency associated with heaving-pitching motion becomes more dominant in the lift (C_L) response, whereas the drag (C_D) exhibits its strongest frequency component at twice the base frequency (2f), especially noticeable at Ψ = 90°. Figure 20(a) highlights a critical shift in the force contribution between the two halves of the motion cycle, beginning at Ψ = 90°, where the roles of drag (C_D) and thrust (C_T) start to reverse. At this phase angle, thrust becomes the primary force over the full cycle and is further amplified at Ψ = 180°, with an increase of approximately 3.7 times, as shown in Fig. 20(b). In terms of lift behaviour, Fig. 21(a)

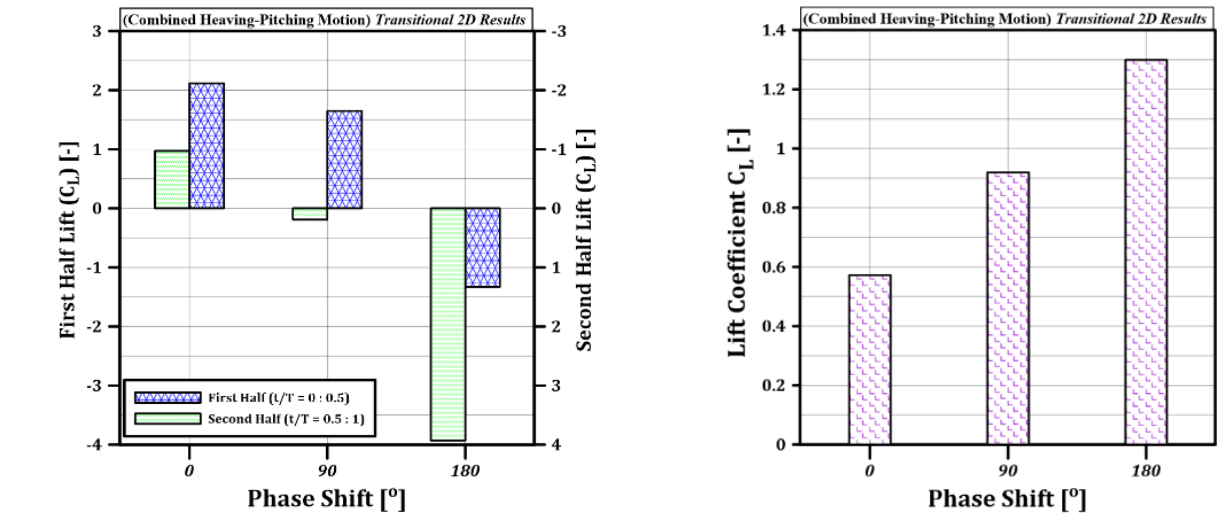

(a) (b)

Fig. 21 (a) Mean lift coefficient (C_L) from each half-cycle and (b) cycle-averaged lift (C_L) at different phase shift angles (Ψ) [Transitional flow]

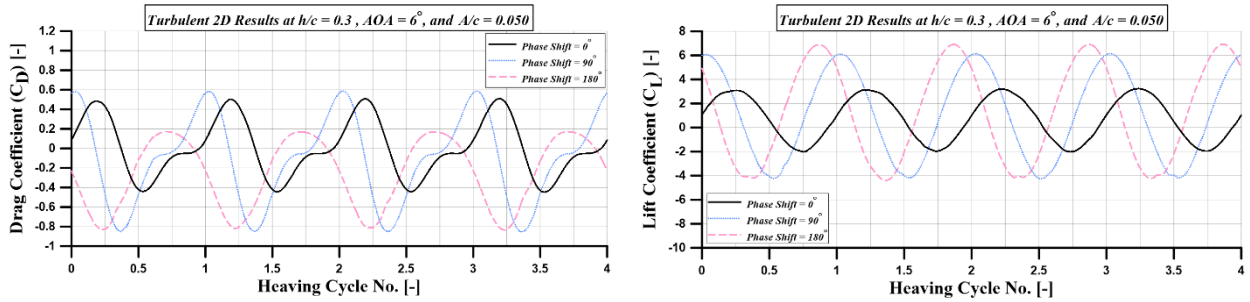

Fig. 22 Aerodynamic force variation for a plunging & pitching WIG configuration at multiple phase shift angles (Ψ) [Turbulent flow]

reveals a notable contrast to the synchronized phase (Ψ = 0°). At Ψ = 180°, both halves of the cycle produce lift (C_L) with opposite signs compared to those at Ψ = 0°, indicating a complete reversal. Interestingly, Ψ = 90° yields positive lift contributions from both halves, and the highest lift per cycle is achieved at Ψ = 180°, as illustrated in Fig. 21(b), with more than double the lift generated under synchronized conditions. These results indicate that by varying the phase-shift angle (Ψ), substantial improvements can be achieved in how a plunging & pitching airfoil performs aerodynamically near the ground.

As shown in Fig. 22, the behaviour of C_D and C_L across various phase shift angles (Ψ) in turbulent flow follows patterns similar to those seen under transitional flow conditions. The key advantage of turbulence, however, lies in its ability to significantly enhance thrust (C_T) near the ground. This is demonstrated in Fig. 23(a), where thrust consistently exceeds drag in the turbulent regime. In contrast, at Ψ = 0° under transitional conditions, drag dominates throughout the cycle. Figure 23(b) reveals that thrust (C_T) increases progressively with larger phase shift angles, reaching a value four times greater at Ψ = 180° compared to Ψ = 0°. At this same phase angle, the thrust generated in turbulent flow exceeds that of transitional flow by approximately 64.9%. Figures 24(a) and 24(b) illustrate lift (C_L) behaviour consistent with transitional flow trends; however, the overall lift is noticeably improved in turbulent flow. For example, at Ψ = 180°, the average lift (C_L) rises by 23.1% relative to its transitional counterpart. In conclusion, turbulent flow conditions substantially improve aerodynamic efficiency, particularly enhancing both C_T and C_L, for airfoils executing heaving-pitching motion in ground effect.

4.3 Effect of Pitching to Heaving (PTH) Frequency Ratio

This section examines how changes in the pitching-to-heaving frequency ratio affect the system, with the heaving frequency held fixed. The pitching-to-heaving (PTH) ratios examined range from 1 to 2. As PTH values increased, mesh deformation became more pronounced, prompting a reduction in the amplitude of heaving to A/c = 0.05. Figure 25 illustrates the formation of vortices around a plunging & pitching airfoil at PTH = 2 under transitional flow. The frames at t/T = 0.25 and 0.75 represent configurations with a consistent total angle of attack (AoA) of 6°. At this frequency ratio, no separation occurred along the lower airfoil surface, and interaction with the ground was minimal. Figure 26 presents the pressure coefficient (C_P) distribution across different PTH ratios and at distinct phases of the heaving-pitching cycle (t/T = 0.25, 0.5, 0.75, and 1). At PTH = 1.5, the aerodynamic response exhibited two alternating force behaviour modes—designated Mode 1 and Mode 2—resulting from the varying total AoA during each half-

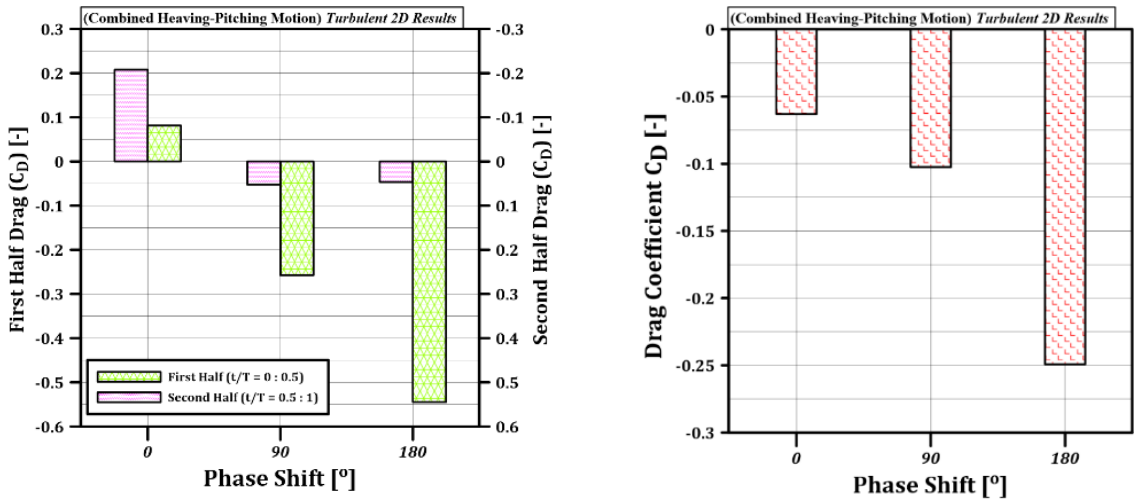

(a) (b)

Fig. 23 (a) Mean impact of each half of the plunging & pitching cycle on drag (C_D) (b) Total drag coefficient (C_D) per cycle at various phase shift angles (Ψ) [Turbulent flow]

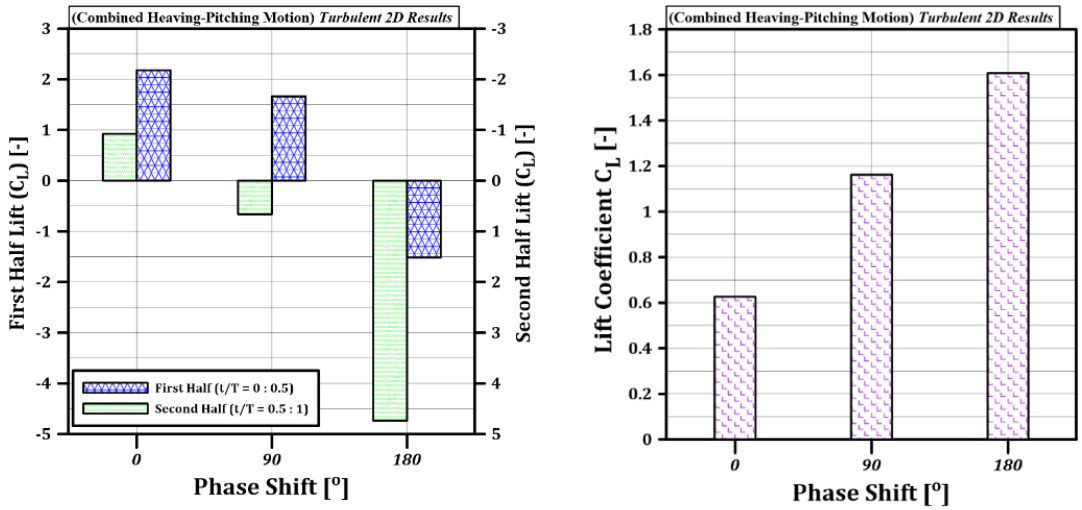

(a) (b)

Fig. 24 (a) Half-cycle contributions to drag coefficient (C_D) and (b) total cycle-averaged drag (C_D) across varying phase shift angles (Ψ) [Turbulent flow]

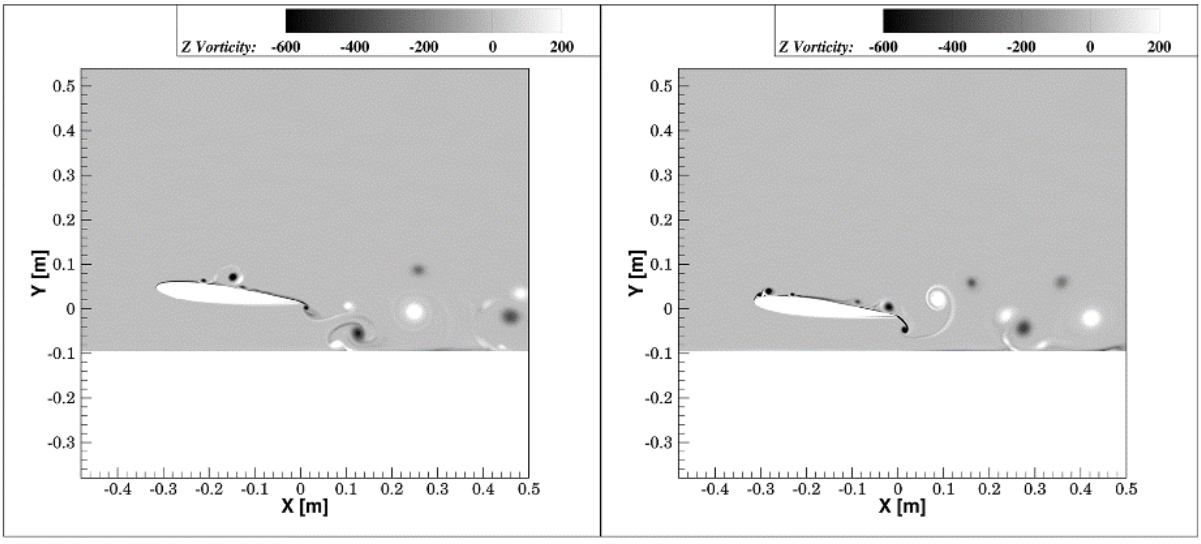

t/T = 0.25 t/T = 0.75

Pitching Freq./Heaving Freq. = 2.0

Fig. 25 Ground interaction with a plunging & pitching wing operating at a pitching-to-heaving frequency ratio (PTH) of 2 [Transitional flow]

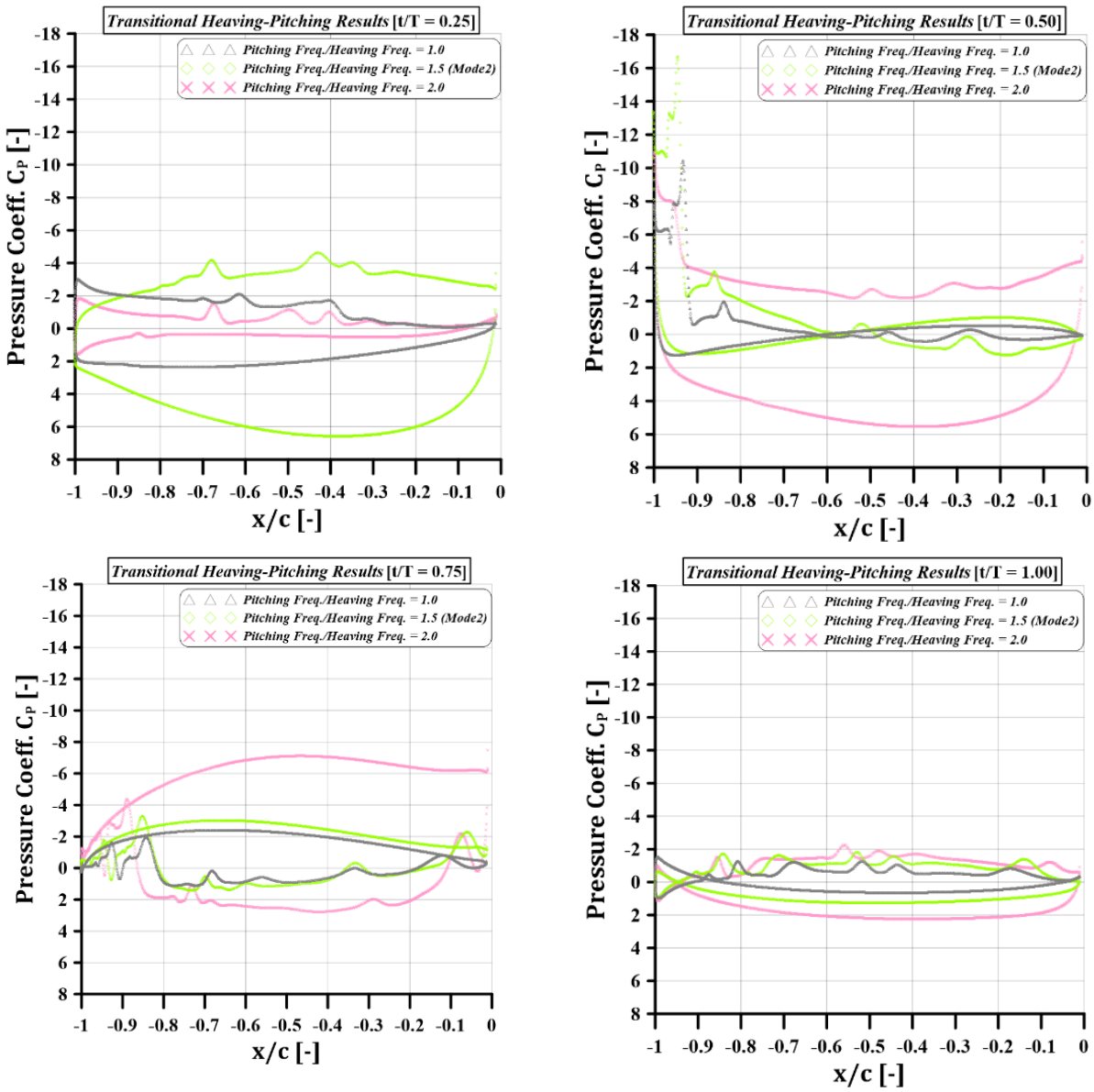

Fig. 26 Distribution of pressure coefficient (C_P) across the wing surface at four stages of the plunging & pitching cycle for varying pitching-to-heaving frequency ratios [Transitional flow]

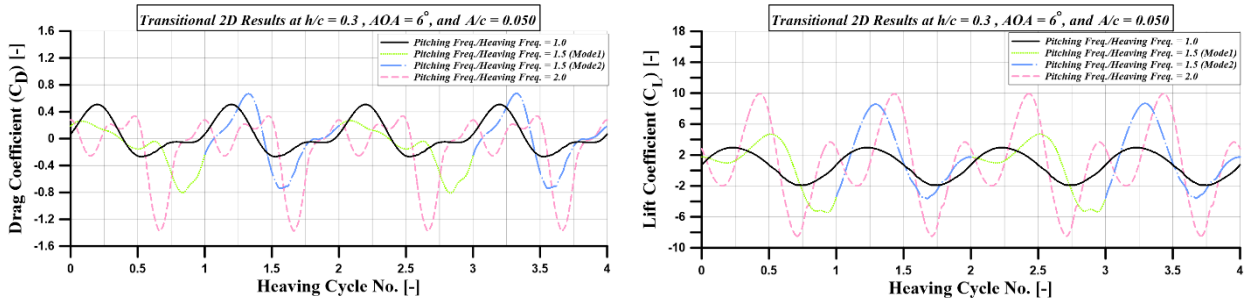

Fig. 27 Aerodynamic force variation for plunging & pitching WIG configuration at different pitching-to-heaving (PTH) frequency ratios under [Transitional flow]

cycle, as shown in Fig. 27. These variations are attributed to differences in airfoil orientation and angular velocity, which produce distinctive C_P patterns across the cycle stages for each PTH case. Thus, only generalized insights can be drawn about the C_L trends at specific instants. At t/T = 0.25 for PTH = 1.5 (Mode 2), a notable asymmetry in C_P across the upper and lower surfaces is observed. This stems from the combined influence of pitch alignment and upward heaving motion, which increases the instantaneous effective AoA enhancing suction on the upper surface and pressure on the lower surface, leading to a peak in lift generation. In contrast, the largest

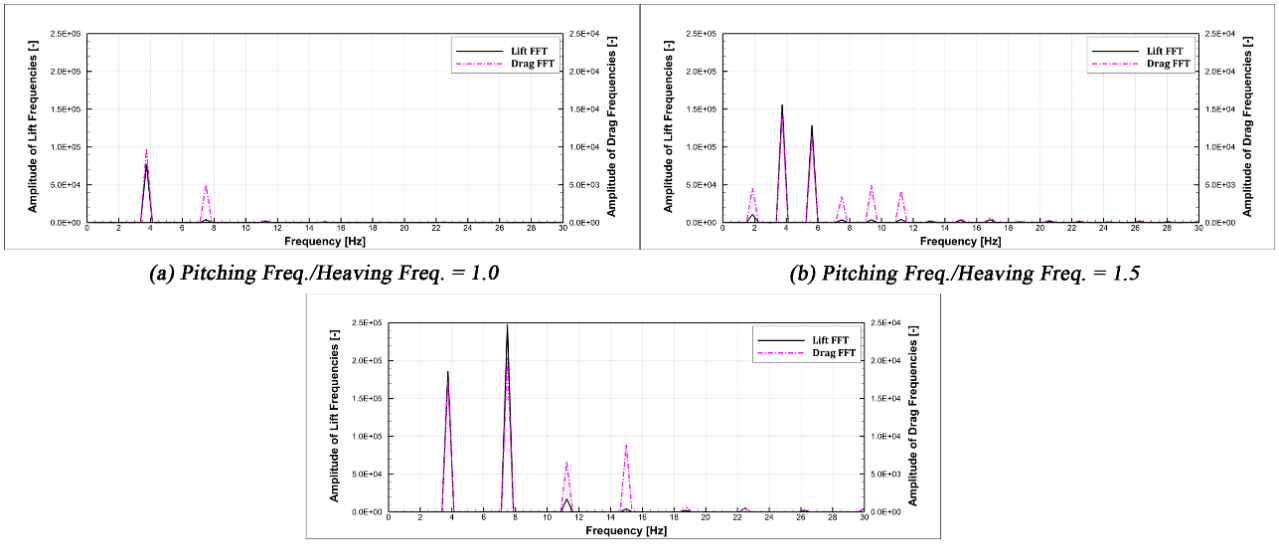

(a) Pitching Freq./Heaving Freq. = 1.0

(b) Pitching Freq./Heaving Freq. = 1.5

(c) Pitching Freq./Heaving Freq. = 2.0

Fig. 28 Frequency analysis of aerodynamic forces for plunging & pitching WIG configuration across varying pitching-to-heaving (PTH) frequency ratios [Transitional flow]

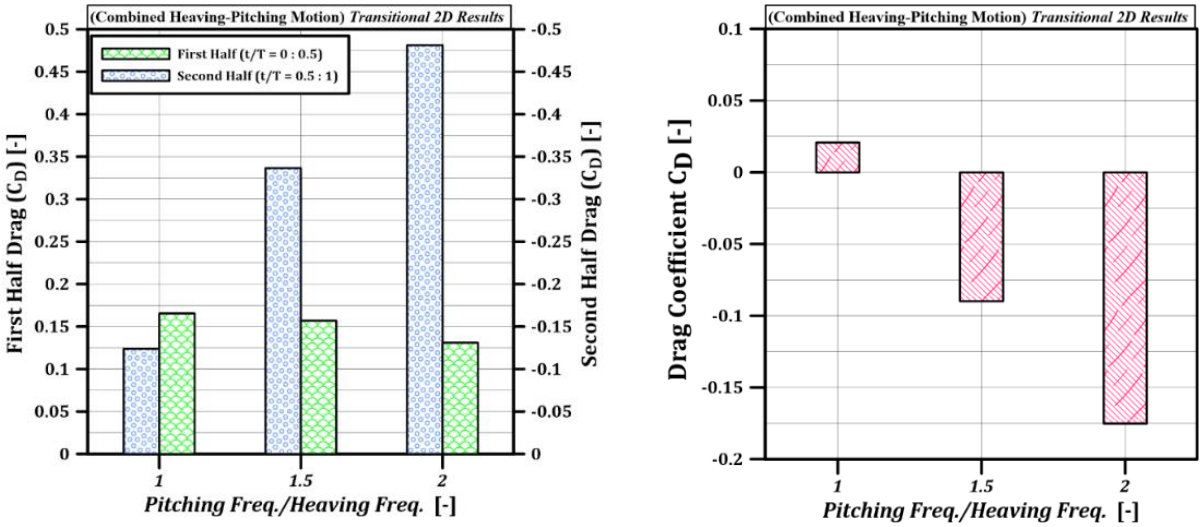

(a) (b)

Fig. 29 (a) Drag coefficient (C_D) contribution from each half-cycle and (b) cycle-averaged drag (C_D) for different pitching-to-heaving (PTH) frequency ratios [Transitional flow]

negative lift ($-C_L$) is expected at t/T = 0.75 for PTH = 2. As illustrated in Fig. 27, the lift coefficient (C_L) patterns support these findings. Additionally, higher PTH ratios correspond to greater fluctuations in lift, while drag (C_D) values trend toward more negative values under these conditions.

Figure 28 displays the results of frequency evaluation of unsteady aerodynamic forces across various pitching-to-heaving (PTH) frequency ratios. At PTH = 1.5, the Fourier breakdown of the lift (C_L) and drag (C_D) coefficients indicate contributions from both heaving and pitching frequencies, with the heaving component being more prominent. Conversely, at PTH = 2, the force coefficients reach their highest amplitudes, primarily influenced by the pitching frequency. Higher-order components corresponding to multiples of both base frequencies are also present, though their magnitudes diminish progressively. As Fig. 29 (a) suggests, drag (C_D) inversely correlates with PTH for t/T = 0:0.5. During the latter half of the cycle, higher PTH values yielded greater thrust (C_T). Based on PTH = 1.5, the net contribution for one heaving-pitching cycle is thrust (C_T), as shown in Fig. 29 (b), almost doubling at PTH = 2. As seen in Fig. 29, increasing the PTH ratio enhances thrust generation due to an imbalance between the drag forces over the cycle where the negative drag in the second half (thrust-producing phase) exceeds the positive drag in the first half. This is driven by favourable C_P distribution and dynamic stagnation point shifts, resulting in a net increase in thrust with higher PTH values. Figure 30(a) shows that as the pitching-to-heaving frequency ratio (PTH) increases, both the negative and positive lift coefficients ($-C_L$ and C_L) grow in magnitude during each half-cycle. However, the difference between them becomes more pronounced, with a stronger contribution from the positive lift (C_L). Figure

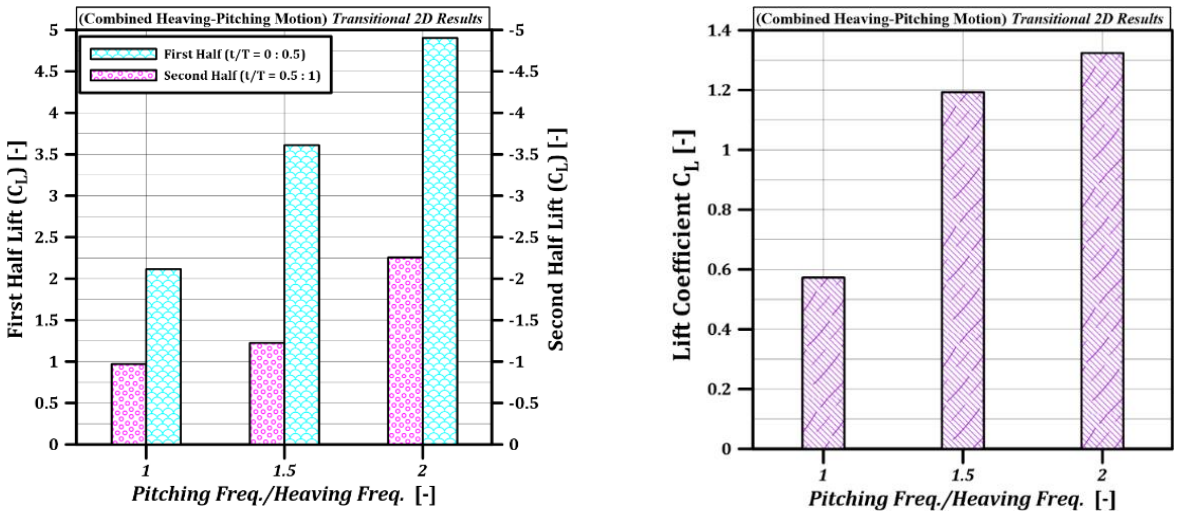

(a) (b)

Fig. 30 (a) Lift coefficient (C_L) contribution from each half-cycle and (b) cycle-averaged lift (C_L) across various pitching-to-heaving (PTH) frequency ratios [Transitional flow]

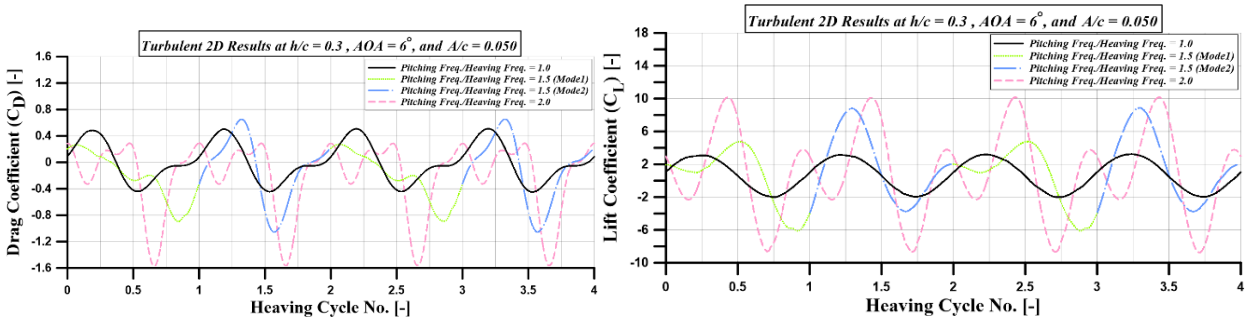

Fig. 31 Aerodynamic force variation for a plunging & pitching WIG configuration at different pitching-to-heaving (PTH) frequency ratios under [Turbulent flow]

30 ((b) shows that at PTH = 2, the lift (C_L) surpasses PTH = 1 by 2.3 times. In Fig. 30(b), the lift coefficient (C_L) at PTH = 2 is approximately 2.3 times higher than at PTH = 1. This results from a greater effective angle of attack and improved phasing between pitch and heave, which intensifies pressure asymmetry and upper surface suction, leading to increased lift. In summary, increasing the pitching-to-heaving (PTH) frequency ratio leads to a notable improvement in the aerodynamic performance of the airfoil.

As shown in Fig. 31, turbulent flow produces stronger and more consistent fluctuations in lift (C_L) and drag (C_D) relative to transitional flow. These fluctuations are more symmetrical and repeatable across cycles, indicating stable vortex shedding and coherent flow structures. In contrast, transitional flow exhibits greater variability and asymmetry, reflecting increased phase sensitivity and less stable aerodynamic behaviour. Throughout the heaving-pitching cycle, changes in pitch angle and vertical velocity cause the effective angle of attack (AoA) to vary continuously, altering the pressure distribution on the airfoil. These variations in AoA lead to corresponding fluctuations in lift (C_L), as shown by the periodic trends observed in Figs. 30 and 31. Higher PTH values intensify the phase difference between pitch and heave motions, leading to sharper variations in the effective angle of attack. This causes stronger pressure differentials across the airfoil, resulting in larger lift (C_L) fluctuations. The intensified unsteady aerodynamic behaviour also promotes faster surface flow, especially during the latter half of the cycle, resulting in greater negative drag (C_D), as illustrated in Figs. 30 and 31. The evolution of the effective angle of attack is governed by the interplay between heaving and pitching frequencies, which in turn directly influences the lift (C_L) and drag (C_D) production. At higher pitch-to-heave ratios (PTH), the altered phase relationship leads to sharper variations in airfoil orientation and relative velocity, which intensify unsteady aerodynamic forces. Consequently, higher PTH values produce larger C_L and C_D fluctuations, with higher peak lift and more negative drag during favourable phases, as demonstrated in Figs. 30 and 31. Figure 32(a) clearly illustrates the drag reduction (C_D) during the first half of the cycle (t/T = 0:0.5) in turbulent flow, which concurrently enhances thrust (C_T) in the latter half. In contrast to transitional flow, turbulent conditions consistently produce thrust across the entire heaving-pitching cycle. As the PTH ratio increases, thrust generation intensifies, as depicted in Fig. 32(b). Specifically, at PTH = 2, the cycle-averaged thrust (C_T) increases nearly four times relative to PTH = 1, with

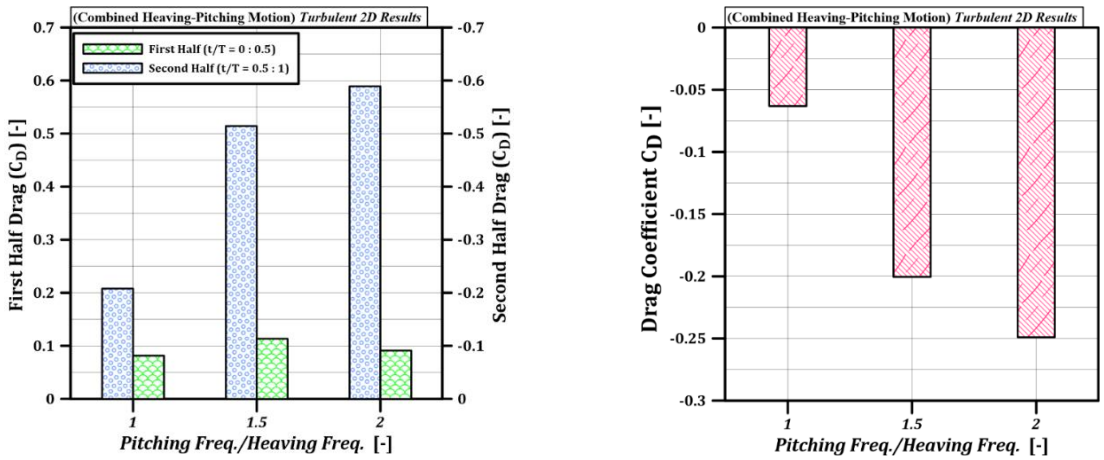

(a) (b)

Fig. 32 (a) Half-cycle contributions to drag coefficient (C_D) and (b) total drag per cycle at various pitching-to-heaving (PTH) frequency ratios [Turbulent flow]

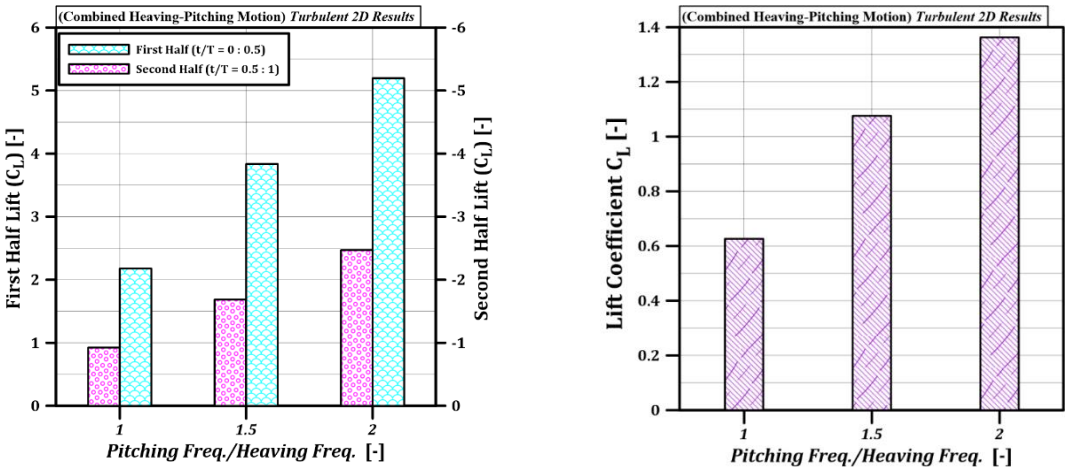

(a) (b)

Fig. 33 (a) Lift coefficient (C_L) contribution from each half of the heaving & pitching cycle and (b) total cycle-averaged lift (C_L) at different pitching-to-heaving (PTH) frequency ratios [Turbulent flow]

turbulent flow yielding a 42.1% gain in thrust relative to transitional flow. As shown in Fig. 32, the enhancement of thrust (C_T) observed in the latter half of the cycle in turbulent flow is due to stronger vortex structures and more efficient momentum transfer near the trailing edge. Turbulence improves flow attachment and vortex coherence, enhancing suction behind the airfoil and sustaining forward thrust throughout the cycle. The pitching-to-heaving (PTH) frequency ratio affects aerodynamic performance by controlling the timing between pitch and heave motions, which modifies the effective angle of attack throughout the cycle. Changes in this timing influence pressure distribution, vortex shedding, and force generation. As shown in Figs. 30 and 32, higher PTH values improve lift and thrust by enhancing flow-structure interaction. In turbulent flow, thrust (C_T) is generated throughout the entire heaving-pitching cycle due to stronger vortex coherence and sustained momentum transfer near the trailing edge. This continuous generation contrasts with transitional flow, where thrust is intermittent. As shown in Fig. 32, turbulence supports more stable flow attachment and efficient conversion of unsteady motion into forward momentum, resulting in persistent thrust. Figure 33 (a) and 33 (b) consistently portray the lift (C_L) behaviour across various flow regimes. Figures 30 and 33 highlight key differences in the aerodynamic behaviour between transitional and turbulent flows. In turbulent conditions, the lift coefficient (C_L) is consistently higher across all PTH values, with increases of approximately 9.4% and 2.9% at PTH = 1 and PTH = 2, respectively, compared to transitional flow. Additionally, turbulent flow maintains continuous thrust (C_T) throughout the cycle, whereas transitional flow exhibits alternating phases of drag and thrust. This indicates that turbulence improves aerodynamic efficiency by sustaining lift and reducing cycle-averaged drag.

5. Conclusions

This research examined the aerodynamic behaviour of a wing-in-ground (WIG) airfoil subjected to simultaneous heaving and pitching motions under both transitional and turbulent flow conditions. The main outcomes and insights derived from the study are as follows:

- Compared to transitional flow, turbulent conditions notably improved the aerodynamic efficiency of the heaving-pitching WIG airfoil, resulting in a 4 to 10 fold increase in thrust across the tested parameter ranges.
- Increasing the pitching angle (Φ) generally reduced the thrust and lift in both flow regimes. The optimal performance was achieved at $\Phi = 2°$, with turbulent flow providing 2.9 times more thrust than transitional flow.
- Adjusting the phase-shift angle (Ψ) amid the heaving and pitching motions substantially improved the aerodynamic characteristics. At $\Psi = 180°$, the thrust increased by 64.9% in the turbulent flow compared with the transitional flow.
- Increasing the frequency ratio of pitching-to-heaving (PTH) motion improves both thrust and lift production. At a PTH value of 2, thrust was four times greater than at PTH = 1, and turbulent flow yielded a 42.1% enhancement in thrust relative to transitional conditions.
- Frequency domain analysis revealed complex interactions between heaving and pitching frequencies in force coefficient oscillations, providing insights into the underlying flow physics.
- The ground effect generally improved aerodynamic performance, with greater thrust and lift observed in proximity to the ground surface.

These results provide valuable insights into optimizing WIG craft design and operation. The study demonstrates that careful tuning of heaving-pitching parameters can significantly enhance aerodynamic efficiency, particularly in turbulent flow conditions. Future work should focus on experimental validation of these numerical findings and exploration of additional parameters to further optimize WIG performance.

CONFLICT OF INTEREST

The authors declare that they have no known competing financial interests or personal relationships that could have appeared to influence the work reported in this paper.

AUTHORS CONTRIBUTION

Y. E. William: Conceptualization, Methodology, Writing- Original draft preparation. **S. Kanagalingam:** Data curation, Writing- Original draft preparation. **M. H. Mohamed*:*** Supervision, Writing- Reviewing and Editing.

AVAILABILITY OF DATA AND MATERIALS:

Data will be made available on request.

REFERENCE

Abate, G., Ol, M., & Shyy, W. (2008). Introduction: Biologically inspired aerodynamics. *AIAA Journal*, *46*(9), 2113–2114. https://doi.org/10.2514/1.35949.

Abdizadeh, G. R., Farokhinejad, M., & Ghasemloo, S. (2022). Numerical investigation on the aerodynamic efficiency of bio-inspired corrugated and cambered airfoils in ground effect. *Scientific Reports*, *12*(1), 19117. https://doi.org/10.1038/s41598-022-23590-2.

Adhikari, D. R., Sargunaraj, M. P., Soto, C. E., Bhattacharya, S., Loubimov, G. E., and Kinzel, M. P. (2020). *Unsteady ground effects on a rectangular and swept wing undergoing heaving and pitching during deceleration. AIAA Scitech 2020 Forum*. Reston, Virginia: American Institute of Aeronautics and Astronautics. https://doi.org/10.2514/6.2020-0334.

Barber, T. J., Leonardi, E., & Archer, R. D. (1999). A technical note on the appropriate CFD boundary conditions for the prediction of ground effect aerodynamics. *The Aeronautical Journal*, *103*(1029), 545–547. https://doi.org/10.1017/s0001924000064368

Barnes, C. J., & Visbal, M. (2016). *High-fidelity LES simulations of self-sustained pitching oscillations on a NACA0012 airfoil at transitional reynolds numbers'. 54th AIAA Aerospace Sciences Meeting*. Reston, Virginia: American Institute of Aeronautics and Astronautics. https://doi.org/10.2514/6.2016-1353.

Ben-Nasr, O. Laurence, D., and Thormann, A. (2017). Assessment of subgrid-scale modeling for large-eddy simulation of a spatially-evolving compressible turbulent boundary layer. *Computers & Fluids*, *151*, 144–158. https://doi.org/10.1016/j.compfluid.2016.07.004

Bertagnolio, F., Sørensen, N. N., & Rasmussen, F. (2005). New insight into the flow around a wind turbine airfoil section1. *Journal of Solar Energy Engineering*, *127*(2), 214–222. https://doi.org/10.1115/1.1861927.

Bleischwitz, R., de Kat, R., & Ganapathisubramani, B. (2016). Aeromechanics of membrane and rigid wings in and out of ground-effect at moderate reynolds numbers. *Journal of Fluids and Structures*, *62*, 318–331. https://doi.org/10.1016/j.jfluidstructs.2016.02.005.

Bleischwitz, R., de Kat, R., & Ganapathisubramani, B. (2017). On the fluid-structure interaction of flexible membrane wings for MAVs in and out of ground-effect. *Journal of Fluids and Structures*, *70*, 214–234. https://doi.org/10.1016/j.jfluidstructs.2016.12.001.

Boudis, A., Bayeul-Laine, A. C., Benzaoui, A., Oualli, H., Guerri, O., and Coutier-Delgosha, O. (2019). Numerical investigation of the effects of nonsinusoidal motion trajectory on the propulsion mechanisms of a flapping airfoil. *Journal of Fluids Engineering*, *141*(4). https://doi.org/10.1115/1.4042175.

Bryant, M., Gomez, J. C., & Garcia, E. (2013). Reduced-order aerodynamic modeling of flapping wing energy harvesting at low reynolds number. *AIAA Journal*, *51*(12), 2771–2782. https://doi.org/10.2514/1.J052364.

Dessi, D., Mastroddi, F., and Mancini, S. (2013). Analytical formulation of 2-D aeroelastic model in weak ground effect. *Journal of Fluids and Structures*, *42*, 270–295. https://doi.org/10.1016/j.jfluidstructs.2013.06.004.

Dominy, R. G. (1992). Aerodynamics of grand prix cars'. *Proceedings of the Institution of Mechanical Engineers, Part D: Journal of Automobile Engineering*, *206*(4), 267–274. https://doi.org/10.1243/PIME_PROC_1992_206_187_02

Gülçat, U. (2013). *Flapping thin airfoil interacting with the ground'*. 3rd South-East European Conference on Computational Mechanics. Kos Island, Greece. https://doi.org/10.7712/130113.4380.S2006

Ito, Y., & Iwashita, H. (2016). Characteristics of unsteady aerodynamics and pressure fields of wings flying with heave motion in the ground effect. *Journal of the Japan Society of Naval Architects and Ocean Engineers*, *24*, 69–83. https://doi.org/10.2534/jjasnaoe.24.69

Jacuzzi, E., & Granlund, K. (2020). Heaving inverted wing in extreme ground effect. *Journal of Fluids Engineering*, *142*(11). https://doi.org/10.1115/1.4047804.

Lee, T., & Lin, G. (2022). Review of experimental investigations of wings in ground effect at low reynolds numbers. *Frontiers in Aerospace Engineering*, *1*. https://doi.org/10.3389/fpace.2022.975158.

Lehmkuhl, O., Baez, A., Rodríguez, I., & Pérez-Segarra, C. D. (2011). *Direct numerical simulation and large-eddy simulations of the turbulent flow around a NACA-0012 Airfoil'. 7th International Conference on Computational Heat and Mass Transfer*. Istanbul, Turkey, pp. 1–8.

Leishman, G. J. (2006). Principles of helicopter aerodynamics with CD extra. 2nd ed. Cambridge University Press, Cambridge, UK. ISBN 978-0-521-85860-1.

Liang, H., Wang, X., Zou, L., and Zong, Z. (2014). Numerical study of two-dimensional heaving airfoils in ground effect. *Journal of Fluids and Structures*, *48*, 188–202. https://doi.org/10.1016/j.jfluidstructs.2014.02.009.

LIIVA, J. (1969). Unsteady aerodynamic and stall effects on helicopter rotor blade airfoil sections. *Journal of Aircraft*, *6*(1), 46–51. https://doi.org/10.2514/3.44000

Lu, H., Lua, K. B., Lim, T. T., and Yeo, K. S. (2014). Ground effect on the aerodynamics of a two-dimensional oscillating airfoil. *Experiments in Fluids*, *55*(7), 1787. https://doi.org/ 10.1007/s00348-014-1787-4.

Molina, J., Zhang, X., & Alomar, A. (2016). Aerodynamics of a pitching and heaving airfoil in ground effect. *AIAA Journal*, *54*(4), 1158–1171. https://doi.org/10.2514/1.J053350.

Molina, J., Zhang, X., & Angland, D. (2011). On the unsteady motion and stability of a heaving airfoil in ground effect. *Acta Mechanica Sinica*, *27*(2), 164–178. https://doi.org/10.1007/s10409-011-0445-9.

Moore, N., Wilson, P. A., & Peters, A. J. (2002). An investigation into wing in ground effect aerofoil geometry. In: Proceedings of the RTO Systems Concepts and Integration Panel Symposium (RTO-MP-095), NATO Research and Technology Organisation.

Moriche, M., Flores, O., & García-Villalba, M. (2017). On the aerodynamic forces on heaving and pitching airfoils at low reynolds number. *Journal of Fluid Mechanics*, *828*, 395–423. https://doi.org/10.1017/jfm.2017.508.

Nicoud, F., & Ducros, F. (1999). Subgrid-scale stress modelling based on the square of the velocity gradient tenso. *Flow, Turbulence and Combustion*, 62(3), 183–200. https://doi.org/10.1023/A:1009995426001

Poirel, D., & Mendes, F. (2014). Experimental small-amplitude self-sustained pitch–heave oscillations at transitional reynolds numbers. *AIAA Journal*, *52*(8), 1581–1590. https://doi.org/10.2514/1.J052541.

Prakash Babu, D. R., Madhesh, D., Hasan, I., & Mukesh, R. (2025). Influence of rough surfaces on airfoil aerodynamics and the ground effect on near-wall flow. *Physics of Fluids*, *37*(2), 023607. https://doi.org/10.1063/5.0252504.

Sarbandi, A., Naderi, A., & Parhizkar, H. (2020). The ground effect on flapping bio and NACA 0015 airfoils in power extraction and propulsion regimes. *Journal of the Brazilian Society of Mechanical Sciences and Engineering*, *42*(6), 287. https://doi.org/10.1007/s40430-020-02376-5

Senturk, U., & Smits, A. J. (2019). Reynolds number scaling of the propulsive performance of a pitching airfoil. *AIAA Journal*, 57(7), 2663–2669. https://doi.org/10.2514/1.J058371.

Shyy, W. (2005). Special issue on animal locomotion in fluids, and its mimicry. *Applied Mechanics Reviews*, *58*(4), 225–225. https://doi.org/10.1115/1.1943432

Shyy, W., Lian, Y., Tang, J., Viieru, D., and Liu, H. (2007). *Aerodynamics of low reynolds number flyers*. Cambridge University Press. https://doi.org/10.1017/CBO9780511551154.

Turkyilmazoglu, M. (2002). The absolute instability of Joukowski-type airfoils. *Theoretical and Computational Fluid Dynamics*, *15*(3), 255–264. https://doi.org/10.1007/s001620100053.

Türkyılmazoglu, M., Gajjar, J. S. B., & Ruban, A. (1999). The absolute instability of thin wakes in an incompressible/compressible fluid. *Theoretical and Computational Fluid Dynamics*, *13*, 91–114. https://doi.org/10.1007/s001620050006.

Versteeg, H. K., & Malalasekera, W. (2007). *An introduction to computational fluid dynamics: The finite volume method* (2nd ed.). Pearson Education. ISBN 978-0-13-127498-3.

Weller, H. G., Tabor, G., Jasak, H., and Fureby, C. (1998). A Tensorial approach to computational continuum mechanics using object-oriented techniques. *Computers in Physics*, *12*(6), 620–631. https://doi.org/10.1063/1.168744.

William, Y. E., Kanagalingam, S., & Mohamed, M. H. (2024). Ground effect investigation on the aerodynamic airfoil behaviour using large eddy simulation. *Journal of Fluids Engineering*, *146*(3). https://doi.org/10.1115/1.4063696.

Wu, J., & Zhao, N. (2013). Ground effect on flapping wing. *Procedia Engineering*, 67, 295–302. https://doi.org/10.1016/j.proeng.2013.12.029

Zerihan, J., & Zhang, X. (2000). Aerodynamics of a single element wing in ground effect. *Journal of Aircraft*, *37*(6), 1058–1064. https://doi.org/10.2514/2.2711

Zhang, X., & Zerihan, J. (2003). Off-surface aerodynamic measurements of a wing in ground effect. *Journal of Aircraft*, 40(4), 716–725. https://doi.org/10.2514/2.3150

Zhi, H., Xiao, T., Deng, S., Tong, M., Chen, P., & Wu, B. (2022). Distinct wing-in-ground effect of airfoil in proximity to water waves. *AIAA Journal*, 60(6), 3789–3804. https://doi.org/10.2514/1.J061216